ministerie van verkeer en waterstaat

koninklijk nederlands meteorologisch instituut

A baroclinic wavy basic state model: description and preliminary experiments

C. J. Kok

wetenschappelijke rapporten WR 87-1

scientific reports WR 87-1

de bilt 1987

CONTENTS

Foreword

In the early 80's the importance of wavy basic state (WBS) barotropic models was demonstrated by various workers. Within the framework of the cooperation between the Cooperative Institute of Climate Studies (CICS) and KNMI the need for a WBS baroclinic model was recognized. At KNMI ideas for such a model had been developed by the author in the beginning of 1983. In 1984 KNMI submitted a research proposal to CICS in which it was proposed to develop, test and conduct preliminary experiments with a two-layer WBS model. This resulted in a subcontract between CICS and KNMI under grant from NOAA (NA84AA-H-00026).

The period of this contract lasted from September 1, 1984 until February 1, 1986. The research was largely carried out at KNMI, with the exception of October and November 1985 when the author visited the University of Maryland.

This report contains a detailed derivation and description of the model as well as the main results of the preliminary experiments.

The research was carried out under the supervision of dr. J.D. Opsteegh.

Part I Description of a baroclinic wavy basic state model

1. Introduction

In this part of the report a technical description is given of a linear baroclinic wavy basic state model for the planetary scales in the atmosphere, i.e. a model in which the equations are linearized around a zonally asymmetric basic state. It is a global 2-layer steady-state model based on the primitive equations. The model variables describe the anomalous zonally asymmetric as well as symmetric circulation in the time-mean atmosphere as a response to prescribed anomalous forcings. The model is semi-spectral: the variables are expressed in wave components in zonal direction, whereas a gridpoint representation is used in meridional direction.

The methodology of the wavy basic state model is similar to that of the 2-layer linear steady-state primitive equations model described by Opsteegh & Van den Dool (1980), hereafter referred to as OD. Apart from the waviness of the basic state these models differ in the fact that the wavy basic state model contains a zonal mean meridional circulation. It also describes anomalies in zonal wavenumber zero as a response to zonal mean forcing as well as zonally asymmetric forcing.

2. Model formulation

The derivation of the model equations is extensively described in Opsteegh & Van den Dool (1980) and will not be repeated here. They arrive at a set of linear equations formulated in terms of the asymmetrical part of the anomalies in the time mean flow. Here these anomaly (or perturbation) equations are also used to calculate the zonally symmetric part of the anomalies. They are expressed in curvilinear coordinates with p as vertical coordinate. With the addition of terms describing the interaction of perturbations with the zonally asymmetric part of the basic state as well as with the climatological zonal mean meridional circulation they are:

Zonal momentum balance

$$U\frac{\partial \hat{u}}{\partial x} + \hat{u}\frac{\partial U}{\partial x} + V\frac{\partial \hat{u}}{\partial y} + \hat{v}\frac{\partial U}{\partial y} + \Omega\frac{\partial \hat{u}}{\partial p} + \hat{\omega}\frac{\partial U}{\partial p} - f\hat{v} + \frac{\partial \hat{\phi}}{\partial x} - U\hat{v}\frac{\tan\phi}{a}$$

$$- V\hat{u}\frac{\tan\phi}{a} + \hat{F}_{W_x} = \hat{F}_{E_x} \qquad (1)$$

Meridional momentum balance

$$U\frac{\partial \hat{v}}{\partial x} + \hat{u}\frac{\partial V}{\partial x} + V\frac{\partial \hat{v}}{\partial y} + \hat{v}\frac{\partial V}{\partial y} + \Omega\frac{\partial \hat{v}}{\partial p} + \hat{\omega}\frac{\partial V}{\partial p}$$

$$+ f\hat{u} + \frac{\partial \hat{\phi}}{\partial y} + 2U\hat{u}\frac{\tan\phi}{a} + \hat{F}_{W_y} = \hat{F}_{E_y} \qquad (2)$$

First law of thermodynamics

$$U\frac{\partial \hat{T}}{\partial x} + \hat{u}\frac{\partial T}{\partial x} + V\frac{\partial \hat{T}}{\partial y} + \hat{v}\frac{\partial T}{\partial y} - \sigma\hat{\omega} + \delta\hat{T} = \frac{\hat{Q}}{c_p} + \hat{Q}_E \qquad (3)$$

Continuity equation

$$\frac{\partial \hat{u}}{\partial x} + \frac{\partial \hat{v}}{\partial y} - \frac{\tan\phi}{a}\hat{v} + \frac{\partial \hat{\omega}}{\partial p} = 0 \qquad (4)$$

Hydrostatic approximation

$$\frac{\partial \hat{\phi}}{\partial p} = -\hat{\alpha} \qquad (5)$$

Equation of state

$$p\hat{\alpha} = R\hat{T} \qquad (6)$$

The basic state, around which the primitive equations are linearized, consists of U, V, Ω, T and σ (static stability). These are functions of height, latitude and longitude, except for σ which depends on latitude only. The model variables for the anomalies (depicted by $\hat{}$) are $\hat{u}$, $\hat{v}$, $\hat{\omega}$, $\hat{T}$, $\hat{\phi}$ and $\hat{\alpha}$. These symbols have their usual meaning. $\hat{F}_{W_x}$, $\hat{F}_{W_y}$ are dissipation terms. These will be discussed below. δ is a Newtonian cooling coefficient. $\hat{F}_{E_x}$, $\hat{F}_{E_y}$ and $\hat{Q}_E$ are the anomalous transient eddy forcing terms of momentum and heat. A description of these terms is given in Kok and Opsteegh (1985). $\hat{Q}$ is the anomalous diabatic heating.

In order to prevent numerical instability small terms proportional to the second derivative with respect to latitude of $\hat{u}$, $\hat{v}$ and $\hat{T}$ have to be added in the zonal and meridional momentum equation and the thermodynamic equation respectively.

Vertical discretization

The vertical discretization of the model is shown in Figure 1. The difference between the isobaric levels can be chosen arbitrarily.

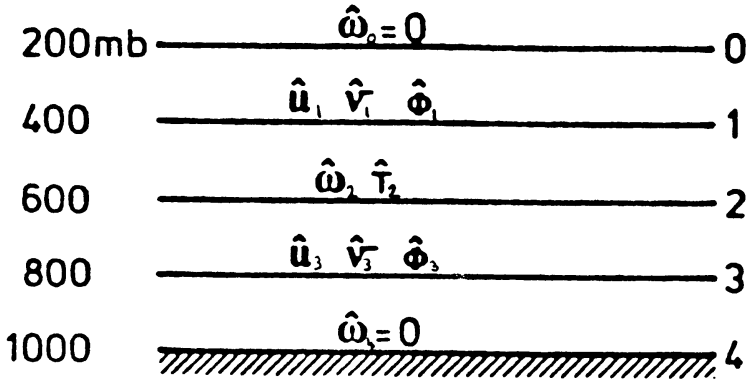

Figure 1

The momentum and continuity equations are applied at levels 1 and 3, whereas the thermodynamic equation is applied at level 2. The hydrostatic approximation and the equation of state are combined to eliminate the anomalous temperature $\hat{T}_2$ in the thermodynamic equation: $\hat{T}_2 = -\frac{P_2}{R}(\frac{\partial \hat{\phi}}{\partial p})_2$.

The model has a rigid upper boundary at 200 mb ($\hat{\omega}_0 = 0$). The lower boundary condition at 1000 mb where the vertical velocity is that produced by the horizontal surface winds over the mountains:

$$\hat{\omega}_4 = -\rho g(U_4 \frac{\partial H}{\partial x} + V_4 \frac{\partial H}{\partial y}) \qquad (7)$$

where ρ is density, g is gravity and H is topographic height. Indices refer to model levels.

The friction terms in the momentum equations have the following form:

$$\begin{aligned}
\hat{F}_{w_{x_1}} &= K_{w_1}\,\hat{u}_1 + K_D(\hat{u}_1 - \hat{u}_3) \\
\hat{F}_{w_{x_3}} &= K_{w_3}\,\hat{u}_3 - K_D(\hat{u}_1 - \hat{u}_3) \\
\hat{F}_{w_{y_1}} &= K_{w_1}\,\hat{v}_1 + K_D(\hat{v}_1 - \hat{v}_3) \\
\hat{F}_{w_{y_3}} &= K_{w_3}\,\hat{v}_3 - K_D(\hat{v}_1 - \hat{v}_3)
\end{aligned} \tag{8}$$

K_w and K_D are the friction and (small) vertical diffusion coefficients respectively. For the time being they are constant in zonal direction.

The vertical derivatives of perturbation quantities

We take

$$\frac{\partial \hat{u}_1}{\partial p} = \frac{\hat{u}_2 - \hat{u}_o}{2\Delta p} = \frac{\hat{u}_2}{2\Delta p} = \frac{\hat{u}_1 + \hat{u}_3}{4\Delta p}$$

$$\frac{\partial \hat{u}_3}{\partial p} = \frac{\hat{u}_4 - \hat{u}_2}{2\Delta p} = -\frac{\hat{u}_2}{2\Delta p} = -\frac{\hat{u}_1 + \hat{u}_3}{4\Delta p}$$

Analogous expressions hold for $\frac{\partial \hat{v}_1}{\partial p}$ and $\frac{\partial \hat{v}_3}{\partial p}$.

$$\frac{\partial \hat{\phi}_2}{\partial p} = \frac{\hat{\phi}_3 - \hat{\phi}_1}{2\Delta p}$$

Finally

$$\frac{\partial \hat{\omega}_1}{\partial p} = \frac{\hat{\omega}_2}{2\Delta p}$$

$$\frac{\partial \hat{\omega}_3}{\partial p} = \frac{\hat{\omega}_4 - \hat{\omega}_2}{2\Delta p} \qquad (9)$$

These latter two discretizations will be used to eliminate $\hat{\omega}_2$ from the equations. With (9) the continuity equations at level 1 and 3 are both equations in $\hat{\omega}_2$:

$$\frac{\partial \hat{u}_1}{\partial x} + \frac{\partial \hat{v}_1}{\partial y} - \frac{\tan\phi}{a}\hat{v}_1 + \frac{\hat{\omega}_2}{2\Delta p} = 0 \qquad (10)$$

$$\frac{\partial \hat{u}_3}{\partial x} + \frac{\partial \hat{v}_3}{\partial y} - \frac{\tan\phi}{a}\hat{v}_3 - \frac{\hat{\omega}_2}{2\Delta p} = -\frac{\hat{\omega}_4}{2\Delta p} \qquad (11)$$

Elimination of $\hat{\omega}_2$ is now obtained by using the sum of (10) and (11) and by substituting $\hat{\omega}_2$ from (10) into the zonal and meridional momentum equations (eq. (1) and (2)) applied at level 1 and into the thermodynamic equation (3), and by subsituting $\hat{\omega}_2$ from eq. (11) into (1) and (2) applied at level 3.

Finally, the vertical derivatives of basic state quantities are written as

$$\frac{\partial U_1}{\partial p} = \frac{U1P}{\Delta p}\ , \text{ etc.}$$

For instance $U1P = \frac{U_3 - U_1}{2}$ and U3P = U1P, etc.

Model equations

Applying the above to eq's (1) to (6) leads to a set of 6 linear equations in the variables $\hat{u}_1$, $\hat{v}_1$, $\hat{\phi}_1$, $\hat{u}_3$, $\hat{v}_3$, $\hat{\phi}_3$:

$$(U_1 - U1P)\frac{\partial \hat{u}_1}{\partial x} + \left(\frac{\partial U_1}{\partial x} + \frac{\Omega_2}{8\Delta p} - \frac{\tan\phi}{a} V_1\right) \hat{u}_1 + V_1 \frac{\partial \hat{u}_1}{\partial y}$$

$$+ \frac{\Omega_2}{8\Delta p} \hat{u}_3 + \left(\frac{\partial U_1}{\partial y} + \frac{\tan\phi}{a} U1p - \frac{\tan\phi}{a} U_1\right) \hat{v}_1 - U1p \frac{\partial \hat{v}_1}{\partial y} \qquad (12)$$

$$+ (K_{w_1} + K_D) \hat{u}_1 - K_D \hat{u}_3 - f\hat{v}_1 + \frac{\partial \hat{\phi}_1}{\partial x} + \mu \frac{\partial^2 \hat{u}_1}{\partial y^2} = \hat{F}_{E_{x_1}}$$

$$-V1P \frac{\partial \hat{u}_1}{\partial x} + \left(\frac{\partial V_1}{\partial x} + 2\frac{\tan\phi}{a} U_1\right)\hat{u}_1 + \left(\frac{\partial V_1}{\partial y} + \frac{\tan\phi}{a} V1P + \frac{\Omega_2}{8\Delta p}\right)\hat{v}_1$$

$$+ U_1 \frac{\partial \hat{v}_1}{\partial x} + \frac{\Omega_2}{8\Delta p} \hat{v}_3 + (V_1 - V1P) \frac{\partial \hat{v}_1}{\partial y} \qquad (13)$$

$$+ (K_{w_1} + K_D) \hat{v}_1 - K_D \hat{v}_3 + f\hat{u}_1 + \frac{\partial \hat{\phi}_1}{\partial y} + \mu \frac{\partial^2 \hat{v}_1}{\partial y^2} = \hat{F}_{E_{y_1}}$$

$$- \frac{\Omega_2}{8\Delta p} \hat{u}_1 + \left(\frac{\partial U_3}{\partial x} - \frac{\Omega_2}{8\Delta p} - \frac{\tan\phi}{a} V_3\right) \hat{u}_3 + (U_3 + U3P) \frac{\partial \hat{u}_3}{\partial x}$$

$$+ V_3 \frac{\partial \hat{u}_3}{\partial y} + \left(\frac{\partial U_3}{\partial y} - \frac{\tan\phi}{a} U3P - \frac{\tan\phi}{a} U_3\right)\hat{v}_3 + U3P \frac{\partial \hat{v}_3}{\partial y} \qquad (14)$$

$$+ (K_{w_3} + K_D) \hat{u}_3 - K_D \hat{u}_1 - f\hat{v}_3 + \frac{\partial \hat{\phi}_3}{\partial x} + \mu \frac{\partial^2 \hat{u}_3}{\partial y^2} = \hat{F}_{E_{x_3}} - \hat{\omega}_4 \frac{U3P}{\Delta p}$$

$$\left(\frac{\partial V_3}{\partial x} + 2\frac{\tan\phi}{a} U_3\right) \hat{u}_3 + V3P \frac{\partial \hat{u}_3}{\partial x} - \frac{\Omega_2}{8\Delta p} \hat{v}_1 + U_3 \frac{\partial \hat{v}_3}{\partial x}$$

$$+ \left(\frac{\partial V_3}{\partial y} - \frac{\tan\phi}{a} V3P - \frac{\Omega_2}{8\Delta p}\right) \hat{v}_3 + (V_3 + V3P) \frac{\partial \hat{v}_3}{\partial y} \qquad (15)$$

$$- K_D \hat{v}_1 + (K_{w_3} + K_D) \hat{v}_3 + f\hat{u}_3 + \frac{\partial \hat{\phi}_3}{\partial y} + \mu \frac{\partial^2 \hat{v}_3}{\partial y^2} = \hat{F}_{E_{y_3}} - \hat{\omega}_4 \frac{V3P}{\Delta p}$$

$$\tfrac{1}{2}\frac{\partial T_2}{\partial x}(\hat{u}_1 + \hat{u}_3) + \tfrac{1}{2}\frac{\partial T_2}{\partial y}(\hat{v}_1 + \hat{v}_3) + \frac{P_2}{2R\Delta p} U_2\left(\frac{\partial \hat{\phi}_1}{\partial x} - \frac{\partial \hat{\phi}_3}{\partial x}\right)$$

$$+ \frac{P_2}{2R\Delta p} V_2\left(\frac{\partial \hat{\phi}_1}{\partial y} - \frac{\partial \hat{\phi}_3}{\partial y}\right) + 2\sigma\Delta p\left(\frac{\partial \hat{u}_1}{\partial x} + \frac{\partial \hat{v}_1}{\partial y}\right) \qquad (16)$$

$$- \frac{2\sigma\Delta p \tan\phi}{a} \hat{v}_1 + \frac{P_2}{2R\Delta p}\delta(\hat{\phi}_1 - \hat{\phi}_3) + \mu \frac{\partial^2}{\partial y^2}(\hat{\phi}_1 - \hat{\phi}_3) = \hat{Q} + \hat{Q}_E$$

$$\frac{\partial \hat{u}_1}{\partial x} + \frac{\partial \hat{u}_3}{\partial x} + \frac{\partial \hat{v}_1}{\partial y} + \frac{\partial \hat{v}_3}{\partial y} - \frac{\tan\phi}{a}(\hat{v}_1 + \hat{v}_3) = -\frac{\hat{\omega}_4}{2\Delta p} \qquad (17)$$

In these equations diffusion terms are added.

Horizontal discretization

All variables, forcings and basic state quantities are expanded in Fourier series along latitude circles, for instance $\hat{u}_1 = \sum_{m=-\infty}^{\infty} \hat{u}_{1m}(\phi) e^{im\lambda}$ with $\hat{u}_{1m}$ complex. Products of (derivatives of) perturbation and basic state quantities are developed in single Fourier series. Details are given in the next section.

In meridional direction we use a gridpoint representation with a resolution of 2.5 degrees of latitude. Central differences are used for derivatives in meridional direction.

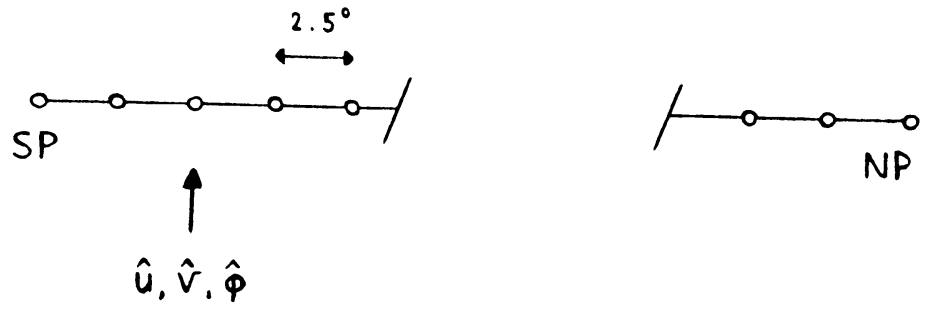

Figure 2

One major disadvantage of the way we discretized the set of equations is that the zonal mean components of the perturbation quantities $\hat{\phi}_1$ and $\hat{\phi}_3$ cannot be solved. This is evident from eqs. (12) - (17) which show that the zonal mean perturbation heights only occur in terms proportional to

$$\frac{\partial}{\partial y}\hat{\phi}_1, \quad \frac{\partial}{\partial y}\hat{\phi}_3 \text{ and } \frac{\partial}{\partial z}(\hat{\phi}_1 - \hat{\phi}_3).$$

This means that we can determine the zonal mean $\hat{\phi}_1$ and $\hat{\phi}_3$ only up to an arbitrary constant which does not depend on latitude and height. Therefore we effectively have 5 instead of 6 zonal mean unknowns (we can for instance replace $\hat{\phi}_1$ and $\hat{\phi}_3$ by $\hat{T}_2$).

Horizontal boundary conditions

In wavenumber zero (m=0) we choose at both poles:

$$\hat{u} = 0$$

$$\hat{v} = 0$$

$$\frac{\partial \hat{\phi}}{\partial y} = 0$$

In m = 1

$$\frac{\partial \hat{u}}{\partial y} = 0$$

$$\frac{\partial \hat{v}}{\partial y} = 0$$

$$\hat{\phi} = 0$$

In $m \geq 2$

$$\hat{u} = 0$$

$$\hat{v} = 0$$

$$\hat{\phi} = 0$$

3. Products of wavy basic state quantities and model variables

In this section we discuss the Fourier expansion along latitude circles of products of (derivatives of) perturbation ($\hat{v}$, e.g.) and known basic state (B) quantities which are themselves expanded in Fourier series. Let

$$\hat{v}(\lambda,\phi) = \sum_{m=-\infty}^{\infty} \hat{v}_m(\phi)e^{im\lambda}$$

$$B(\lambda,\phi) = \sum_{m=-\infty}^{\infty} B_m(\phi)e^{im\lambda}$$

B_m and $\hat{v}_m$ are complex coefficients depending on latitude ϕ (and on vertical coordinate p), λ is longitude.

$$\hat{v}_{-m} = \overline{\hat{v}}_m$$

$$B_{-m} = \overline{B}_m \tag{18}$$

in which the overbar denotes the complex conjugate. The caret, ^, will be omitted form now on.

Only terms like Bv and $B\frac{\partial v}{\partial x}$ are discussed. All products of a model variable and a basic state quantity appearing in the model equations (12) to (17) can be reduced to terms proportional to these forms by using the discretization in y or p direction.

$$Bv = \left(\sum_{-\infty}^{\infty} B_m e^{im\lambda}\right)\left(\sum_{-\infty}^{\infty} v_m e^{im\lambda}\right) = \sum_{\ell=-\infty}^{\infty} \gamma_\ell e^{i\ell\lambda} \tag{19a}$$

$$\text{with} \quad \gamma_\ell = \sum_{k=-\infty}^{\infty} B_{\ell-k} v_k \tag{19b}$$

It follows, making use of (18), that

$$\gamma_{-\ell} = \sum_{k=-\infty}^{\infty} B_{-\ell-k} v_k = \sum_{k=-\infty}^{\infty} B_{-\ell+k} v_{-k} = \sum_{k=-\infty}^{\infty} \overline{B}_{\ell-k} \overline{v}_k = \overline{\gamma}_\ell \qquad (20)$$

indicating that the coefficients of the expansion of Bv in negative powers can simply be obtained from those belonging to positive powers. Therefore we consider only the Fourier series of Bv for $\ell > 0$ (Bv_+). We separate the complex coefficients into real and imaginary parts denoted by subscripts r and i respectively.

$$(Bv)_+ = \sum_{\ell=0}^{\infty} \gamma_\ell e^{i\ell\lambda} = \sum_{\ell=0}^{\infty} \{ \sum_{k=-\infty}^{\infty} B_{\ell-k} v_k \} e^{i\ell\lambda}$$

$$= \sum_{\ell=0}^{\infty} B_\ell v_0 e^{i\ell\lambda} + \sum_{\ell=0}^{\infty} \sum_{k=1}^{\infty} \{ B_{\ell-k} v_k + B_{\ell+k} v_{-k} \} e^{i\ell\lambda}$$

$$= \sum_{\ell=0}^{\infty} (B_{\ell r} + iB_{\ell i}) v_{or} e^{i\ell\lambda}$$

$$+ \sum_{\ell=0}^{\infty} [\sum_{k=1}^{\infty} \{ (B_{(\ell-k)r} + iB_{(\ell-k)i})(v_{kr} + iv_{ki}) + (B_{(\ell+k)r} + iB_{(\ell+k)i})(v_{-kr} + iv_{-ki}) \}] e^{i\ell\lambda}$$

$$= \sum_{\ell=0}^{\infty} (B_{\ell r} + iB_{\ell i}) v_{or} e^{i\ell\lambda}$$

$$+ \sum_{\ell=0}^{\infty} [\sum_{k=1}^{\infty} \{ (B_{(\ell-k)r} + B_{(\ell+k)r}) v_{kr} + (-B_{(\ell-k)i} + B_{(\ell+k)i}) v_{ki} \}$$

$$+ i \sum_{k=1}^{\infty} \{ (B_{(\ell-k)i} + B_{(\ell+k)i}) v_{kr} + (B_{(\ell-k)r} - B_{(\ell+k)r}) v_{ki} \}] e^{i\ell\lambda}$$

$$= \sum_{\ell=0}^{\infty} (B_{\ell r} + iB_{\ell i}) v_{or} e^{i\ell\lambda} \qquad (21)$$

$$+ \sum_{\ell=0}^{\infty} [\sum_{k=1}^{\infty} \{ (B_{(k-\ell)r} + B_{(k+\ell)r}) v_{kr} + (B_{(k-\ell)i} + B_{(k+\ell)i}) v_{ki} \}] e^{i\ell\lambda}$$

$$+ i \sum_{\ell=1}^{\infty} [\sum_{k=1}^{\infty} \{ (-B_{(k-\ell)i} + B_{(k+\ell)i}) v_{kr} + (B_{(k-\ell)r} - B_{(k+\ell)r}) v_{ki} \}] e^{i\ell\lambda}$$

In the latter expression $\ell = 0$ is omitted in the imaginary part.

A similar expression can be obtained for terms of the form $B\frac{\partial v}{\partial x}$. Again only the positive part of the Fourier expansion is considered.

With $v = \sum_m v_m e^{im\lambda}$, $v_m = v_{mr} + iv_{mi}$ it follows that (with R is the earth radius)

$$\frac{\partial v}{\partial x} = \frac{1}{R\cos\phi}\frac{\partial v}{\partial \lambda} = \frac{1}{R\cos\phi}\sum_m imv_m e^{im\lambda} = \sum_m\{(\frac{\partial v}{\partial x})_{mr} + i(\frac{\partial v}{\partial x})_{mi}\}e^{im\lambda}$$

Thus

$$(\frac{\partial v}{\partial x})_{mr} = \frac{-m}{R\cos\phi} v_{mi}$$

$$(\frac{\partial v}{\partial x})_{mi} = \frac{m}{R\cos\phi} v_{mr}$$

Substituting $\frac{1}{R\cos\phi}(-kv_{ki}, kv_{kr})$ for (v_{kr}, v_{ki}) in (21) therefore gives the expression for $(B\frac{\partial v}{\partial x})_+$:

$$(B\frac{\partial v}{\partial x})_+ = \frac{1}{R\cos\phi}\sum_{\ell=o}^{\infty}[\sum_{k=1}^{\infty}k\{(B_{(k-\ell)i} + B_{(k+\ell)i})v_{kr} - (B_{(k-\ell)r} + B_{(k+\ell)r})v_{ki}\}]e^{i\ell\lambda}$$

$$+ i.\frac{1}{R\cos\phi}\sum_{\ell=1}^{\infty}[\sum_{k=1}^{\infty}k\{(B_{(k-\ell)r} - B_{(k+\ell)r})v_{kr} + (B_{(k-\ell)i} - B_{(k+\ell)i})v_{ki}\}]e^{i\ell\lambda} \quad (22)$$

4. Numerical Organization

All terms in the model equations (12) to (17) - including the r.h.s. terms - can now be written in Fourier series along latitude circles. The negative powers of the expansion do not have to be taken into account so the system of equations just has to be solved for zonal wavenumbers $\ell = 0$, until ℓmax only. For each wavenumber the equations are separated in real and imaginary parts.

For each gridpoint the system can be written in the form $M\vec{x} = \vec{F}$, or rather,

$$M_{\ell j}\,\vec{x}_j = \vec{F}_\ell \qquad (23)$$

with ℓ and $j = 0, \ldots, \ell$max.

$\vec{F}_\ell$ is the forcing vector in wavenumber ℓ, consisting of subvectors $\vec{F}_{or}, \vec{F}_{1r}, \vec{F}_{1i}, \ldots, \vec{F}_{(\ell max)r}, \vec{F}_{(\ell max)i}$. $\vec{x}_j$ is the perturbation vector consisting of subvectors $\vec{x}_{or}, \vec{x}_{1r}, \vec{x}_{1i}, \ldots, \vec{x}_{(\ell max)i}$. Each subvector contains the appropriate real or imaginary component of the model variables $u_1, u_3, v_1, v_3, \phi_1, \phi_3$ for wavenumber j, i.e.

$$\vec{x}_{jr} = (u_{1r}^{(j)}, u_{3r}^{(j)}, v_{1r}^{(j)}, v_{3r}^{(j)}, \phi_{1r}^{(j)}, \phi_{3r}^{(j)})$$

$$\vec{x}_{ji} = (u_{1i}^{(j)}, u_{3i}^{(j)}, v_{1i}^{(j)}, v_{3i}^{(j)}, \phi_{1i}^{(j)}, \phi_{3i}^{(j)})$$

Each subvector of $\vec{F}_\ell$ and $\vec{x}_j$ has 6 NRP elements, with NRP is the number of gridpoints between the poles.

$M_{\ell j}$ is an "interaction" matrix which determines the contribution to $\vec{x}_j$ from forcing in zonal wavenumber ℓ. If the waviness of the basic state is

excluded all elements of $M_{\ell j}$, $\ell = j$ are zero. Then the set of equations can be solved for each zonal wave separately. This was the case in OD. If the basic state is asymmetric the system has to be solved for all wavenumbers combined.

Separated in submatrices and subvectors (23) has the following form (for $\ell max = 2$):

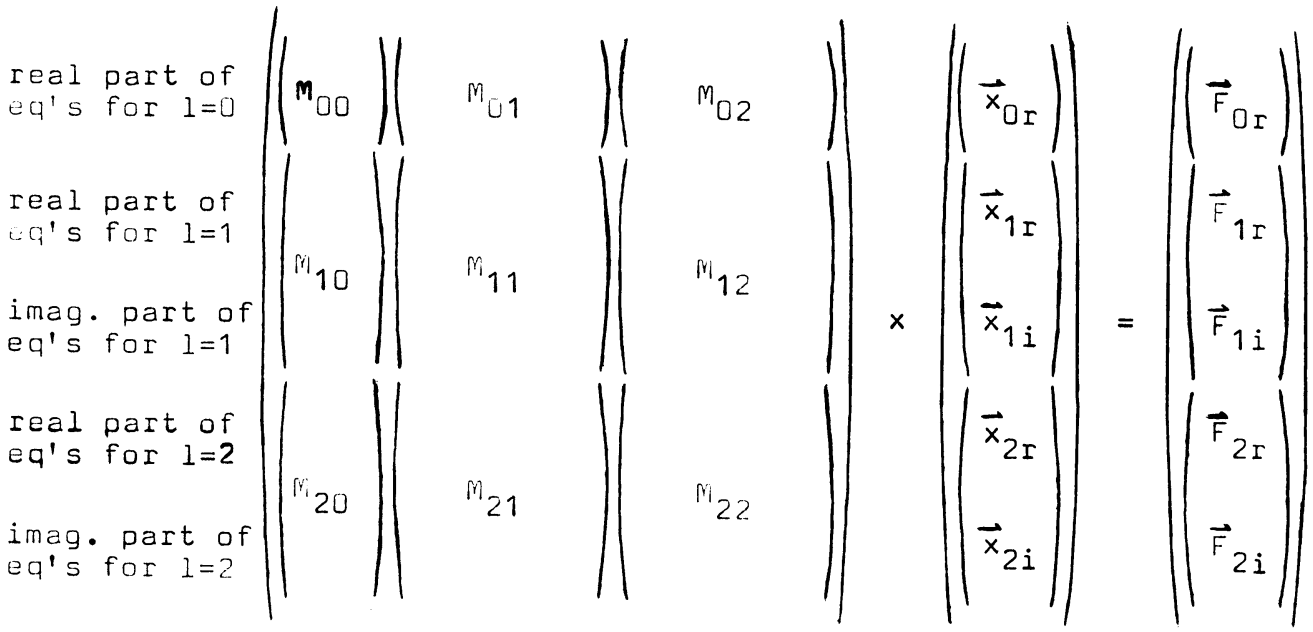

Figure 3

The interaction matrices M_{ij} contain terms proportional to the basic state quantities B_k and B_ℓ with $k - j = i$

and $\ell + j = i$.

All linear terms are contained in M_{ii}, $i = 0, \ldots, \ell max$.

The choice of ℓmax determines which Fourier coefficients of the basic state have to be taken into account in solving the equations. These coefficients are, as can be seen from (21) or (22) (with summations

truncated at ℓmax and using that the number of variables kmax = the number of equations ℓmax):

$$B_{(1-\ell max)r},\ B_{(1-\ell max)i},\ \cdots,\ B_{(2\ell max)r},\ B_{(2\ell max)i}$$

For numerical purposes they have to be assigned to an array number (also dependent on ℓmax):

$$B(1),\ \ldots,\ B(6\ell max).$$

This means that

$$B_{mr} \rightarrow B(2\ell max - 1 + 2m)$$

$$B_{mi} \rightarrow B(2\ell max + 2m).$$

The same transformation is made for the model variables. With these transformations (21) becomes

$$(Bv)_+ = \sum_{\ell=0}^{\ell max} \{B(2\ell max-1+2\ell)+iB(2\ell max+2\ell)\}v(2\ell max-1)e^{i\ell\lambda}$$

$$+ \sum_{\ell=0}^{\ell max}\Big[\sum_{k=1}^{\ell max}\{(B(2\ell max-1+2k-2\ell)+B(2\ell max-1+2k+2\ell))v(2\ell max-1+2k)$$

$$+(B(2\ell max+2k-2\ell)+B(2\ell max+2k+2\ell))v(2\ell max+2k)\}\Big]e^{i\ell\lambda}$$

$$+ i\sum_{\ell=1}^{\ell max}\Big[\sum_{k=1}^{\ell max}\{(-B(2\ell max+2k-2\ell)+B(2\ell max+2k+2\ell))v(2\ell max-1+2k)$$

$$+ (B(2\ell max-1+2k-2\ell)-B(2\ell max-1+2k+2\ell))v(2\ell max+2k)\}\Big]e^{i\ell\lambda}$$

$$= \sum_{\ell=0}^{\ell max} \{B(2\ell max-1+2\ell)+iB(2\ell max+2\ell)\}v(2\ell max-1)e^{i\ell\lambda}$$

$$+ \sum_{\ell=0}^{\ell max}\Big[\sum_{\substack{k=2\ell max+2\\ k\ even}}^{4\ell max}\{B(k-1-2\ell)+B(k-1+2\ell)\}v(k-1)$$

$$+\sum_{\substack{k=2\ell max+2\\ k\ even}}^{4\ell max}\{B(k-2\ell)+B(k+2\ell)\}v(k)\Big]e^{i\ell\lambda}$$

$$+ i\sum_{\ell=1}^{\ell max}\Big[\sum_{\substack{k=2\ell max+2\\ k\ even}}^{4\ell max}\{-B(k-2\ell)+B(k+2\ell)\}v(k-1)$$

$$+\sum_{\substack{k=2\ell max+2\\ k\ even}}^{4\ell max}\{B(k-1-2\ell)-B(k-1+2\ell)\}v(k)\Big]e^{i\ell\lambda}$$

$$= \sum_{\ell=0}^{\ell max} \{B(2\ell max-1+2\ell)+iB(2\ell max+2\ell)\}v(2\ell max-1)e^{i\ell\lambda}$$

$$+ \sum_{\ell=0}^{\ell max}\Big[\sum_{k=2\ell max+1}^{4\ell max}\{B(k+2\ell)+B(k-2\ell)\}v(k)\Big]e^{i\ell\lambda}$$

$$+ i\sum_{\ell=1}^{\ell max}\Big[\sum_{\substack{k=2\ell max+1\\ k\ oneven}}^{4\ell max-1}\{B(k+1+2\ell)-B(k+1-2\ell)\}v(k)$$

$$+\sum_{\substack{k=2\ell max+2\\ k\ even}}^{4\ell max}\{-B(k-1+2\ell)+B(k-1-2\ell)\}v(k)\Big]e^{i\ell\lambda}. \qquad (24)$$

In the same manner (22) becomes

$$\left(B\frac{\partial v}{\partial x}\right)_{+} = \sum_{\substack{\ell=o \\ k\ oneven}}^{\ell max}\Bigg[\sum_{k=2\ell max+1}^{4\ell max-1}\frac{k-2\ell max+1}{2R\cos\phi}\{B(k+1+2\ell)+B(k+1-2\ell)\}v(k)$$

$$-\sum_{\substack{k=2\ell max+2 \\ k\ even}}^{4\ell max}\frac{k-2\ell max}{2R\cos\phi}\{B(k-1+2\ell)+B(k-1-2\ell)\}v(k)\Bigg]e^{i\ell\lambda}$$

$$+\ i\sum_{\ell=1}^{\ell max}\Bigg[\sum_{\substack{k=2\ell max+1 \\ k\ oneven}}^{4\ell max-1}\frac{k-2\ell max+1}{2R\cos\phi}\{-B(k+2\ell)+B(k-2\ell)\}v(k)$$

$$-\sum_{\substack{k=2\ell max+2 \\ k\ even}}^{4\ell max}\frac{k-2\ell max}{2R\cos\phi}\{B(k+2\ell)-B(k-2\ell)\}v(k)\Bigg]e^{i\ell\lambda} \qquad (25)$$

This can also be obtained from (24) by replacing

$v(k)$ by $-\frac{k-2\ell max+1}{2R\cos\phi}\,v(k+1)$ if k is odd

$v(k)$ by $\frac{k-2\ell max}{2R\cos\phi}\,v(k-1)$ if k is even.

From the last two expressions it is easy to determine in which column MII of the matrix M the coefficients belonging to terms proportional to Bv and $B\frac{\partial v}{\partial x}$ have to be placed.

Recall that $v(2\ell max-1)$ corresponds to v_{or},

$v(2\ell max+1)$ v_{1r},

$v(2\ell max+2)$ v_{1i}, etc.

and $v_{1r} = (u_{1r}^{(1)}, u_{3r}^{(1)}, v_{1r}^{(1)}, v_{3r}^{(1)}, \phi_{1r}^{(1)}, \phi_{3r}^{(1)}$, etc.

If we further define IVAR = 1 for $v = u_{1r}$ and $v = u_{1i}$

IVAR = 2 for $v = u_{3r}$ and $v = u_{3i}$

.

.

IVAR = 6 for $v = \phi_{3r}$ and $v = \phi_{3i}$

then the coefficients of v(k) in eqs. (24) and (25) should be placed in the matrix in column MII = $6(k-2\ell max)$ + IVAR if $k > 2\ell max+1$.

If $k = 2\ell max-1$ then MII = IVAR. The position of terms in the equations which are not proportional to Bv or $B\frac{\partial v}{\partial x}$ is trivial.

The rows of the matrix are filled with the real and imaginary parts of the equations (in the order of (12) to (17)) for wavenumbers 0 until &max. This is depicted on the left in Fig. 3. Our system of 6(2&max+1) linear equations for each gridpoint is solved with a matrix-technique described by Lindzen and Kuo (1967) and Simmons (1981).

5. Continuity of the basic state

The wavy basic state has to fulfill the continuity equation. If we assume, as we did in section 2, that

$$\left(\frac{\partial\Omega}{\partial p}\right)_1 = \frac{\Omega_2}{2\Delta p} \text{ and } \left(\frac{\partial\Omega}{\partial p}\right)_3 = \frac{\Omega_4-\Omega_2}{2\Delta p} \text{ then}$$

$$\frac{\partial U_1}{\partial x} + \frac{\partial V_1}{\partial y} - \frac{\tan\phi}{a}V_1 + \frac{\Omega_2}{2\Delta p} = 0 \qquad (26)$$

$$\frac{\partial U_3}{\partial x} + \frac{\partial V_3}{\partial y} - \frac{\tan\phi}{a}V_3 - \frac{\Omega_2}{2\Delta p} = -\frac{\Omega_4}{2\Delta p} \qquad (27)$$

One possible way to meet these requirements is to derive the U and V fields at level 1 from observations. Then (26) can be used to calculate Ω_2.

The inbalance that results in the l.h.s. of (27) if we also obtain U_3 and V_3 from observations can be attributed to Ω_4, which does not show up in the model.

An alternative way is to derive Ω_2 from

$$\frac{\partial}{\partial x}(U_1 - U_3) + \frac{\partial}{\partial y}(V_1 - V_3) - \frac{\tan\phi}{a}(V_1 - V_3) + \frac{\Omega_2}{\Delta p} = \frac{\Omega_4}{2\Delta p} \qquad (28)$$

Part II. Preliminary experiments

1. Introduction

In order to test the wavy basic state (WBS) model a few experiments have been performed. The experiments are chosen in such a way that the results can be compared qualitatively with similar experiments with barotropic WBS models and models with a zonally symmetric basic state. In all cases an anomalous diabatic heating of an elliptical shape is used at 600 mb with a maximum of 3.9 K/day. The position of this heat forcing will be shifted with respect to basic states of various meridional and longitudinal complexity. In most experiments also results are shown for the zonally symmetric case, in order to emphasize the differences between the WBS model and the zonally symmetric model described by Opsteegh and van den Dool (1981).

Only geopotential height responses at 400 mb are shown, in one case accompanied by the response in the same field at 800 mb. For reasons stated in section I.2 the response in zonal wavenumber zero (m = 0) is not included in the figures. However, forcing in the zonal mean component does contribute to this zonally asymmetric response.

All pictures consist of m = 1 until 6 only. The inclusion of higher wavenumbers did not have a noticeable effect on the results in this set of experiments. In all experiments the basic state vertical velocity was calculated from the basic state (zonal and meridional) wind fields using the continuity equation as described in § I.5. Unless otherwise stated the linear friction coefficients were chosen to be rather small in order to emphasize remote effects of the heat forcings. At the top level (400 mb) this coefficient is 10^{-7} s^{-1}, whereas at the bottom level (800 mb) it is 10^{-6} or 2×10^{-6} s^{-1}. The value of the Newtonian cooling coefficient is in all cases 4×10^{-7} s^{-1}.

In all but the last experiment we will use basic states which are modifications of the idealized northern hemisphere (NH) wintertime zonally averaged basic state consisting of zonal winds and temperature only. Between 30°N and 30°S the idealized zonal winds are described by

$$U_1 = 8.5 + 13.5 \cos (6\phi - \pi) \text{ (m/s)}$$
$$U_2 = \frac{2}{3} U_1 - 0.5$$
$$U_3 = \frac{1}{3} U_1 - 1.0$$

Poleward of 30° zonal winds at all levels decrease exponentially with latitude to a value of about 1 m/s near the poles. The zonally averaged temperatures at 600 mb are given by

$$T_2 = 255.5 + 18.5 \cos 2\phi$$

In the last experiment we have taken the three-dimensional observed normal January basic state consisting of m = 0 to 6 of zonal and meridional winds and temperatures at the appropriate levels.

2. Experiments

Experiment 1

In the first experiment (Fig. 4) we consider the remote midlatitude response to an elliptically shaped heating at two locations on the equator. The basic state outside an equatorial strip between 10°S and 10°N is the (idealized) equivalent barotropic Northern Hemispheric wintertime zonally symmetric basic state consisting of zonal winds and temperature only. This idealized basic state is described in section II.1. Meridional winds are taken equal to zero. The zonal winds in the equatorial strip also have a zonal wavenumber one component. Its amplitude is chosen in such a way that a tropical "duct" in which the winds are westerly, is created between 120°E and 120°W at all model levels. The easterlies are hatched in the figure. This basic state is adopted in both hemispheres.

In Fig. 4a the equatorial heating is centered at 0° longitude and lies almost completely within the belt of easterlies. In Fig. 4b the heating is centered at the dateline. The midlatitude geopotential height response at 400 mb (given in decameters) differs by a factor of four between the two cases. Since the background flow is exactly the same outside the latitudes of the forcing this difference is solely due to differences in the basic state at the locations of the forcing itself. This behaviour of the WBS model is consistent with the fact that meridional energy propagation is suppressed by the presence of local easterlies. Increasing the latitudinal extent of the easterlies in the vicinity of the heating leads to a zero response at midlatitudes.

This experiment shows the importance of incorporating zonal structure in the basic state. Taking only the zonally symmetric part can be highly insufficient for assessing the stationary midlatitudinal effects of tropical heat sources.

Experiment 2

In the second experiment - displayed in Fig. 5 - we will study the remote effects of a heating which is located at midlatitudes. In this experiment we use exactly the same basic state as in experiment 1. For comparison we also show the response for the zonally symmetric case (Fig. 5a). The heating is located between 25°N and 45°N and centered at 150°E in Fig. 5a and b. Comparison between these two figures shows that if the tropical zonally asymmetric basic state includes a duct in which the winds are westerly energy can easily propagate from one hemisphere to the other. It appears that only waves of zonal scale less than the zonal scale of the westerly duct can reach the opposite hemisphere. That's why the response in middle and high latitudes of the southern hemisphere in Fig. 5b is strongly dominated by m=3. Its amplitude is highly determined by the strength of the westerlies in the equatorial duct. (Note the different isoline distance in the southern hemisphere.) This can be understood in terms of the dispersion characteristics of forced Rossby waves. It can be shown that the horizontal group velocity of the disturbance increases rapidly with the westerly wind speed (see e.g. Hoskins and Karoly, 1981). So if the westerly winds in the duct are weak the perturbation will be dissipated before it reaches the strong westerlies in the southern hemisphere.

The cross-equatorial propagation appears largest if the centre of the forcing is located approximately 30 degrees to the west of the centre of the duct (displayed in Fig. 5b). Since in our case the duct has a width of 120° a shift of the forcing of approximately 60° in longitude will lead to almost exactly the opposite response at high latitudes in the southern hemisphere. This is shown in Fig. 5c and d in which the centres of the heating in the NH are located at longitudes 130°E and 180°E respectively. The amplitude and phase of the response in the NH is hardly affected by the loss of perturbation energy to the SH.

If the forcing is located at longitudes with easterlies to the south then the response is constrained to lie poleward of the source and there will be hardly any cross-equatorial energy propagation. These situations resemble the zonally symmetric case depicted in Fig. 5a.

The above-mentioned results are in excellent agreement with earlier studies by Webster and Holton (1982) and Branstator (1983). Webster and

Holton obtained their results with a nonlinear model based on the shallow water equations with a time-mean wavy basic state zonal wind field. Branstator used a steady barotropic model linearized around a basic state which varied in latitude and longitude. The vertical structure we used in our experiments 1 and 2 is equivalent barotropic.

Experiment 3

In experiment 3 we will study the effects of the relative position of midlatitude troughs and ridges of the basic state with respect to a wavetrain excited by an equatorial heating. We adopt the same zonally symmetric component of the basic state as in the previous experiments, except equatorward of 10° N where we assume weak westerly winds of 5 m/s at all levels in order to obtain appreciable remote responses. Only north of 15° N the zonal wind field includes a zonal wavenumber one. The vertical structure is again equivalent barotropic. The amplitude of m = 1 is 1 m/s at 400 mb, 0.75 m/s at 600 mb and 0.5 m/s at 800 mb. We shift this wavy basic state in eastern direction in steps of 60 degrees and consider the responses to the equatorial heating which is fixed between 30 and 90°E again (Fig. 6b to 6g). Longitudes at which the zonal winds are strongest are indicated by an upward directed arrow at the bottom of each panel. For comparison also the response is shown in case the zonal structure of the basic state is absent (Fig. 6a).

A number of interesting features can be noticed. First of all in all figures a wavetrain can be seen originating from the area of the forcing following a route up to 70°N and extending all the way around the hemisphere. There is also an indication of a second wavetrain to the south. Comparing Fig. 6b to Fig. 6g it is evident that the distance between two consecutive extrema in the 400 mb geopotential height is smallest when the local background flow reaches its smallest value.

This results can be compared with the ray tracing analysis of Hoskins and Karoly (1981). They applied kinematic wave theory and ideas from geometrical optics to the linearized nondivergent barotropic vorticity equation on the sphere. They showed that, using a Mercator projection of the sphere, along a wave ray the "stationary wavenumber", $m^2 + l^2$, is equal to $\beta_M / \bar{U}_M$. Here m and l are zonal and

meridional wavenumber respectively, β_M is cosϕ times the meridional gradient of the absolute vorticity on the sphere, and $\bar{U}_M$ is the Mercator basic zonal velocity. Therefore the wavelength of the stationary wave will increase (decrease) with increasing (decreasing) local zonal winds.

Although the analysis by Hoskins and Karoly was for zonally symmetric basic states one still can apply their results to models with zonally varying basic states provided that these longitudinal variations are small. (This was shown e.g. by Branstator, 1983.) Since our basic state consists of m = 0 and a small amplitude m = 1 the above-mentioned theory can be applied to our experiment and indeed qualitatively explains the general features of the response.

This experiment exhibits a new phenomenon, not found in the earlier experiments. For in this experiment there appears a strong enhancement of the midlatitude response at distances very far from the equatorial source if this source is located at certain positions with respect to the phase of the basic state zonal wavenumber one. This is most apparent in Fig. 6g, in which the amplitude on the western hemisphere is a factor of 3 larger than in the smallest amplitude case (Fig. 6c) .

So not only the path taken by the energy is affected by the background flow, as was shown in the previous experiments, but apparently it can also provide an additional source of energy for the midlatitude pattern. The importance of the interaction between perturbation wave and basic state was shown earlier by Simmons (1982), Branstator (1983) and others.

Shifting the phase of the m = 1 wave of the zonal flow from 120° (Fig. 6c) to 360° (Fig. 6g) shows a gradual amplification of the remote response, indicating an increasing amount of energy being extracted from the zonal flow. From 360° to 120° a more abrupt decline in amplitude is noticeable. Maximum values of the geopotential height perturbations always occur about 90° west of the longitude of the maximum winds with the exception that the area between 0° and 100°E appears to be hardly affected by changes in the background flow. In this area the equatorial heat anomaly presumably is the primary source of energy.

Comparing finally the asymmetric cases with the symmetric one (Fig. 6a) it appears that the amplitudes are larger in all cases with zonal asymmetry with the exception of Fig. 6c. This case resembles the symmetric one most.

Experiment 4

In the previous experiments we have taken basic states with very simple horizontal and vertical structure. Horizontally it consisted of zonal winds of zonal wavenumbers 0 an 1 only, zonally symmetric temperatures and no meridional winds . Basic state vertical velocities were calculated using the continuity equation for the basic state quantities (§ I.5). In all cases the vertical structure of the zonal winds was equivalent barotropic: maximum winds occurred at the same longitudes at all levels. It is not surprising that the structure of the remote responses showed a predominant equivalent barotropic structure in all cases (not shown).

In this final experiment we take the observed normal January basic state consisting of m = 0 until m = 6 of zonal and meridional winds at 400, 600 and 800 mb, and temperatures at 600 mb. Basic state vertical velocities are calculated by means of the continuity equation again. The linear friction coefficient at the top level is 10^{-6}, at the bottom level 2×10^{-6}. We will study the responses for several locations of an equatorial heating.

In Fig. 7 the 400 and 800 mb basic state zonal winds are displayed in the way they are used in this experiment. At both levels on the NH the winds present strong zonal asymmetries. In the top panel the midlatitude jetstreams can be recognized. The Asian or Pacific jet is the strongest one with windspeeds exceeding 40 m/s. A second jet is located over the south of the United States. It is smaller and weaker than the Asian jet. Another local maximum in the zonal winds is noticeable over North Africa. In large parts of the equatorial region the winds are easterly. The SH shows much less zonal structure.

First we show the geopotential height responses at 400 and 800 mb to an elliptically shaped equatorial heating between 0 and 60°W after the zonal asymmetries in the basic state are removed (Fig. 8a and b). A wavetrain is evident, in particular at 400 mb (top panel), with rapidly decreasing amplitude following the ray. It is restricted to longitudes up to some 100 degrees downstream of its source. The amplitudes are rather small because in this zonally symmetric case most of the heating is embedded in an easterly background flow. This is especially true for the SH. The vertical structure of the anomalies is baroclinic close to

the source and equivalent barotropic at more remote distances. This is well known from numerous studies with zonally symmetric models.

In Fig. 9 the m = 1 to 6 geopotential height responses at 400 mb are shown when the waviness of the basic state is included. In Fig. 10 the corresponding fields at 800 mb are displayed. The longitudinal extent of the equatorial heating is indicated on top of each panel.

The most conspicuous feature in Fig. 9 is the almost complete insensitivity of the structure of the NH midlatitude response to the longitudinal position of the tropical heating. Placing its centre anywhere in the region ranging from 90°E eastward to about 90°W the midlatitude response only differs in amplitude and hardly at all in phase (Fig. 9 b,c,d,e). Even outside this region the responses are reminiscent of this pattern. Apparently the normal January basic state in the way we used it appears to have a stationary mode that can be very easily excited.

Highest values occur when the centre of the heating lies near the centre of the Pacific (Fig. 9d). Note that the response is large even in the case when the northern hemispheric part of the heating lies almost completely in a region with local easterlies (Fig. 9c).

Similar behaviour was noted by Simmons et al (1983) who found that their barotropic model, linearized about the climatological January 300 mb flow, also possessed regions of preferred response to tropical as well as subtropical forcings. Structures which resemble the observed Pacific North America (PNA) pattern noted by Wallace and Gutzler (1981) tended to recur in their responses. The areas of preferred response correspond to places where the perturbation waves can extract energy from the basic state most efficiently.

We can also compare our results with those obtained from a similar experiment performed with a GCM by Blackmon et al (1983). In their experiment an anomalous sea-surface temperature (SST) with the distribution of Rasmusson and Carpenter's (1982) El Nino-Southern Oscillation composite (but with twice its amplitude) was introduced into the NCAR Community Climate Model (CCM). Our recurring northern hemispheric pattern of Fig. 9 resembles to some degree the asymmetric part of their anomalous 1200-day average 200 mb height field. The main differences are that their anomalous pattern lies more to the south and the height anomaly near 50°W 75°N is missing.

Geisler et al (1985) found that the structure of the CCM midlatitude response to tropical Pacific SST anomalies is rather independent of the longitudinal position of the anomalies. Branstator (1985) could not reproduce this finding with his barotropic model linearized about the CCM 500 mb wavy basic state. Our results indicate that a model linearized about the full three-dimensional January basic state is capable of reproducing the insensitivity of the response to the location of the forcing. However, this insensitivity appears to be far too large in comparison with the results of Geisler et al. Apparently our normal mode is extremely dominant, i.e. there is one eigenvalue with a much larger growth rate than all others.

It is interesting to note that if the heating is located south of the very weak parts of the subtropical jet the NH midlatitude responses are small (Fig. 9a, f) whereas strong responses occur when the heating lies south of the Asian or North American jet. This agrees with earlier findings of for instance Simmons (1982) and Navarra (1985) who also found strong enhancements of midlatitude responses when the heating was located closely to the main jet streams.

The above-mentioned phenomena for the NH can to a much lesser extent be noticed in the southern hemispheric midlatitudes also. However, the most important difference is the much smaller amplitude of the responses in the SH. Since the basic state has much less longitudinal variation in this hemisphere (Fig. 7) the responses do not exhibit as much enhancement with respect to the zonally symmetric case depicted in Fig. 8.

In Fig. 10 the geopotential height responses at the bottom level are shown for the same positions of the anomalous heating. Again the NH midlatitude amplitude is by far the largest. Comparison with Fig. 9 shows a predominant barotropic structure with highest values occurring in general at the top level. However, there are a few striking exceptions. Over the Northern Pacific and North America there are also places where the response is highly baroclinic. This is regardless of the distance to the heating. The possibility of baroclinic remote responses is a typical feature of wavy basic state models which are not be encountered in zonally symmetric models.

3. Summary

In this part of the report a description is given of a few experiments performed with the steady state baroclinic wavy basis state model (described in part I). Only responses to isolated anomalous heatings are considered. The position of these heat forcings has been shifted with respect to basic states of various meridional and longitudinal complexity.

The experiments show that incorporating zonal structure in the basic state at the location of the heating can be very important. Taking only the zonally symmetric part can be highly insufficient for assessing the stationary midlatitudinal effects of tropical heat sources.

Incorporating in the tropics a longitudinally asymmetric basic state which includes a duct in which the zonal winds are westerly, can have a large influence on the cross-equatorial propagation of forced waves. It is shown that waves of zonal scales less than the zonal scale of the westerly duct may propagate from one hemisphere to the other. The amplitude of the response in one hemisphere to forcing in the opposite hemisphere depends strongly on the magnitude of the westerlies in the equatorial duct. It is also found that in case of zonally symmetric basic state zonal winds and temperature the cross-equatorial propagation can be affected by the inclusion in the basic state of (zonally symmetric or asymmetric) meridional winds in the tropics. This latter result has not been discussed in section II.2.

The ray tracing analysis of Hoskins and Karoly (1981) for zonally symmetric barotropic basic states can also be applied to equivalent barotropic basic states which contain small longitudinal variations. For instance the wavelength of the stationary wave is strongly dependent on the amplitude of the local background flow.

Another important feature apparent from the experiments is that the background flow can provide an additional source of energy by interacting with the perturbation waves. This is most evident in the experiment in which we studied the responses to a heating which was placed at various locations along the equator using the three-dimensional normal January basic state. Apart from the large amplitudes that occur in some cases in the northern hemisphere the most conspicuous phenomenon in this experiment is the almost complete insensitivity of

the structure of the northern hemisphere midlatitude response to the position of the equatorial heating. Apparently the January basic state possesses a stationary mode that can be excited very easily.

Acknowledgement

This research was supported by NOAA under grant NA84AA-H-00026 and was partly carried out at the University of Maryland. The author would like to thank his colleagues Robert Mureau for his valuable discussions during the early stages of the development of the model and Theo Opsteegh and Fons Baede for carefully reading the manuscript. He also greatly appreciates the help of Birgit Kok and Loes Tonneman for typing the manuscript.

References.

Blackmon, M.L., J.E. Geisler and E.J. Pitcher, 1983: A general circulation model study of January climate anomaly patterns associated with interannual variation of equatorial Pacific sea-surface temperatures. J. Atmos. Sci., 40, 1410-1425.

Branstator, G.W., 1983: Horizontal energy propagation in a barotropic atmosphere with meridional and zonal structure. J. Atmos. Sci., 40, 1689-1708.

Branstator, G.W., 1985: Analysis of general circulation model sea-surface temperature anomaly simulations using a linear model. Part I: Forced solutions. J. Atmos. Sci., 42, 2225-2241.

Geisler, J.E., M.L. Blackmon, G.T. Bates and S. Munoz, 1985: Sensitivity of January climate response to the magnitude and postion of equatorial Pacific sea-surface temperature anomalies. J. Atmos. Sci., 42, 1037-1049.

Hoskins, B.J. and D.J. Karoly, 1981: The steady linear response of a spherical atmosphere to thermal and orographic forcing. J. Atmos. Sci., 38, 1179-1196.

Kok, C.J. and J.D. Opsteegh, 1985. Possible causes of anomalies in seasonal mean circulation patterns during the 1982-1983 El Nino event. J. Atmos., Sci., 42, 677-694.

Lindzen, R.S. and H.L. Kuo, 1969. A reliable method for the numerical integration of a large class of ordinary and partial differential equations. Mon. Wea. Rev., 96, 732-734.

Navarra, A., 1985: Anomaly general circulation models. Ph.D. Thesis Geophysical Fluid Dynamics Laboratory, Princeton, NJ.

Opsteegh, J.D. and H.M. van den Dool, 1980. Seasonal differences in the stationary response of a linearized primitive equation model: Prospects for long range weather forecasting? J. Atmos. Sci., 37, 2169-2185.

Rasmusson, E.M. and T.H. Carpenter, 1982: Variations in tropical sea-surface temperature and surface wind fields associated with the Southern Oscillation, Mon. Wea. Rev., 110, 354-384.

Simmons, A.J., 1982: The forcing of stationary wave motion by tropical heating. Quart. J.R. Met. Soc.,108, 503-534.

Simmons, A.J., J.M. Wallace and G.W. Branstator, 1983: Barotropic wave propagation and instability, and atmospheric teleconnection patterns. J. Atmos. Sci., 40, 1363-1392.

Wallace, J.M. and D.S. Gutzler, 1981: Teleconnection in the geopotential height field during the Northern Hemisphere winter. Mon. Wea. Rev., 109, 785-812.

Webster, P.J. and J.R. Holton, 1982: Cross equatorial response to middle latitude forcing in a zonally varying basic state. J. Atmos. Sci., 39, 722-733.

Figure captions (part II)

Fig. 4 Geopotential height response at 400 mb to an anomalous heating centered at the equator at longitudes 0° (a) and 180° (b). The elliptically shaped heating is indicated by the dashed-dotted lines. The basic state is described in the text. The areas where the zonal winds are easterly are hatched.

Fig. 5 As in Fig. 4, except that the centers of the anomalous heatings are located at 35°N and at longitudes 150°E (a and b), 130°E (c) and 180° (d) respectively.

Fig. 6 Geopotential height response at 400 mb to an anomalous equatorial heating located between 30° and 90° E when the basic state is zonally symmetric (a) and when the zonal winds of the basic state also have a m=1 component which is shifted in eastward direction in steps of 60 degrees (b to g). Longitudes at which the zonal winds are strongest are indicated by an arrow at the bottom of each panel.

Fig. 7 Observed normal January zonal winds (m = 0 until 6) at 400 mb (a) and 800 mb (b).

Fig. 8 Geopotential height response at 400 mb (a) and 800 mb (b) to an anomalous heating located at the equator between 0° and 60° W, using only the zonally symmetric part of the normal January climatology.

Fig. 9 Geopotential height responses at 400 mb for six positions of the equatorial heating (which are indicated on top of each panel). The three-dimensional normal January basic state is used.

Fig. 10 As in Fig. 9 but for 800 mb.

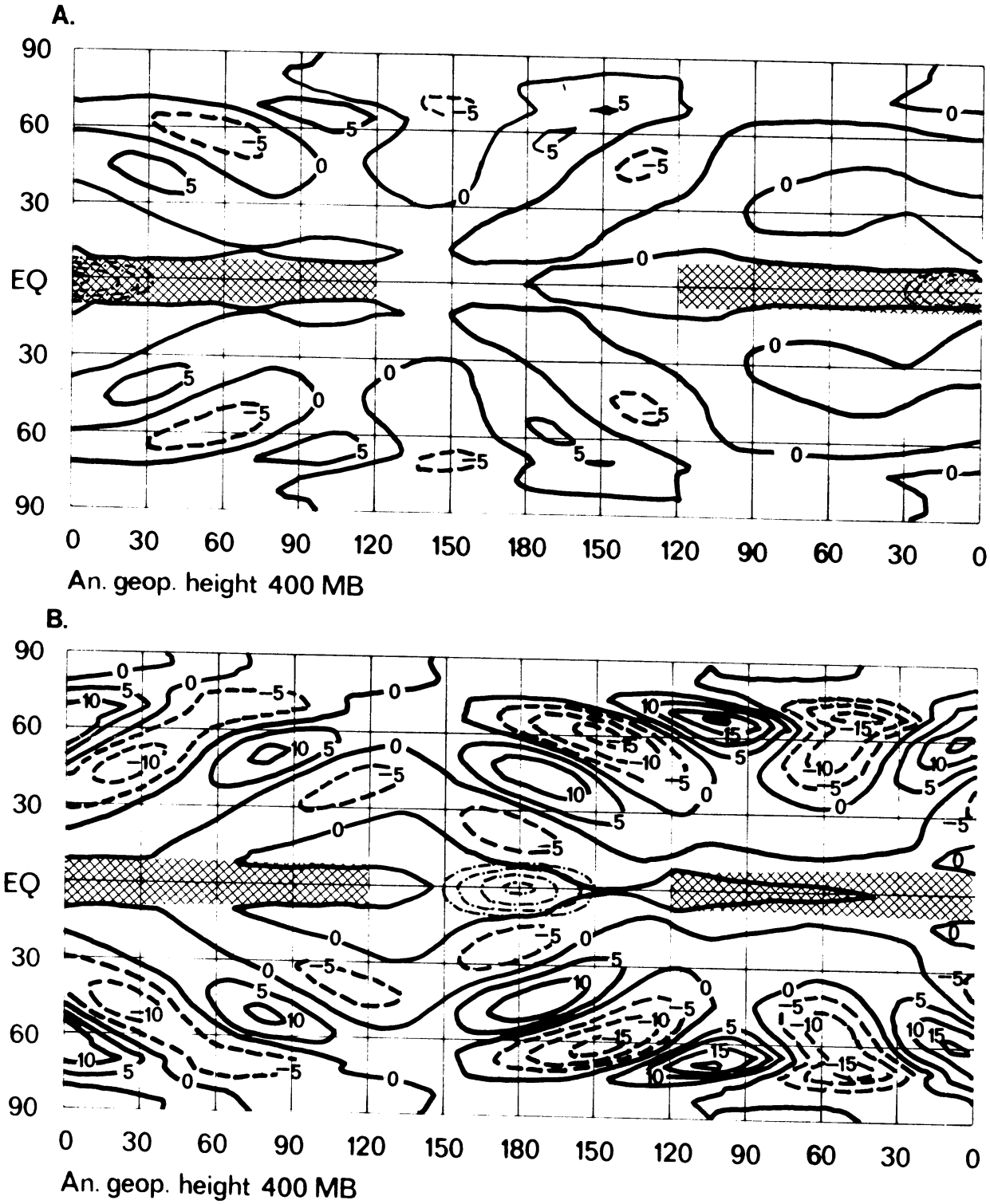
A.
90
60
30
EQ
30
60
90
0 30 60 90 120 150 180 150 120 90 60 30 0
An. geop. height 400 MB
B.
90
60
30
EQ
30
60
90
0 30 60 90 120 150 180 150 120 90 60 30 0
An. geop. height 400 MB

Fig. 4

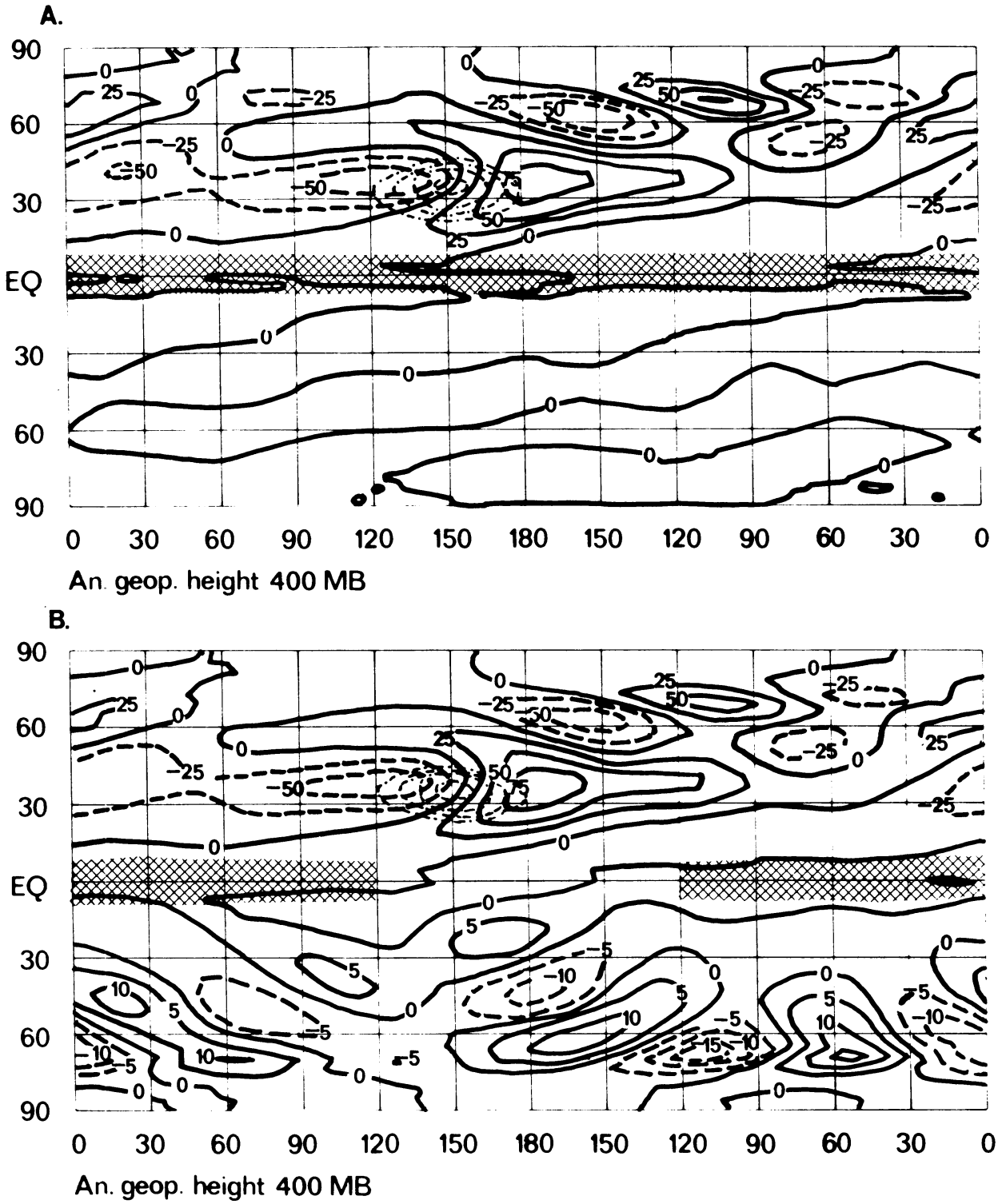
A.
90
60
30
EQ
30
60
90
0 30 60 90 120 150 180 150 120 90 60 30 0
An. geop. height 400 MB
B.
90
60
30
EQ
30
60
90
0 30 60 90 120 150 180 150 120 90 60 30 0
An. geop. height 400 MB

Fig. 5

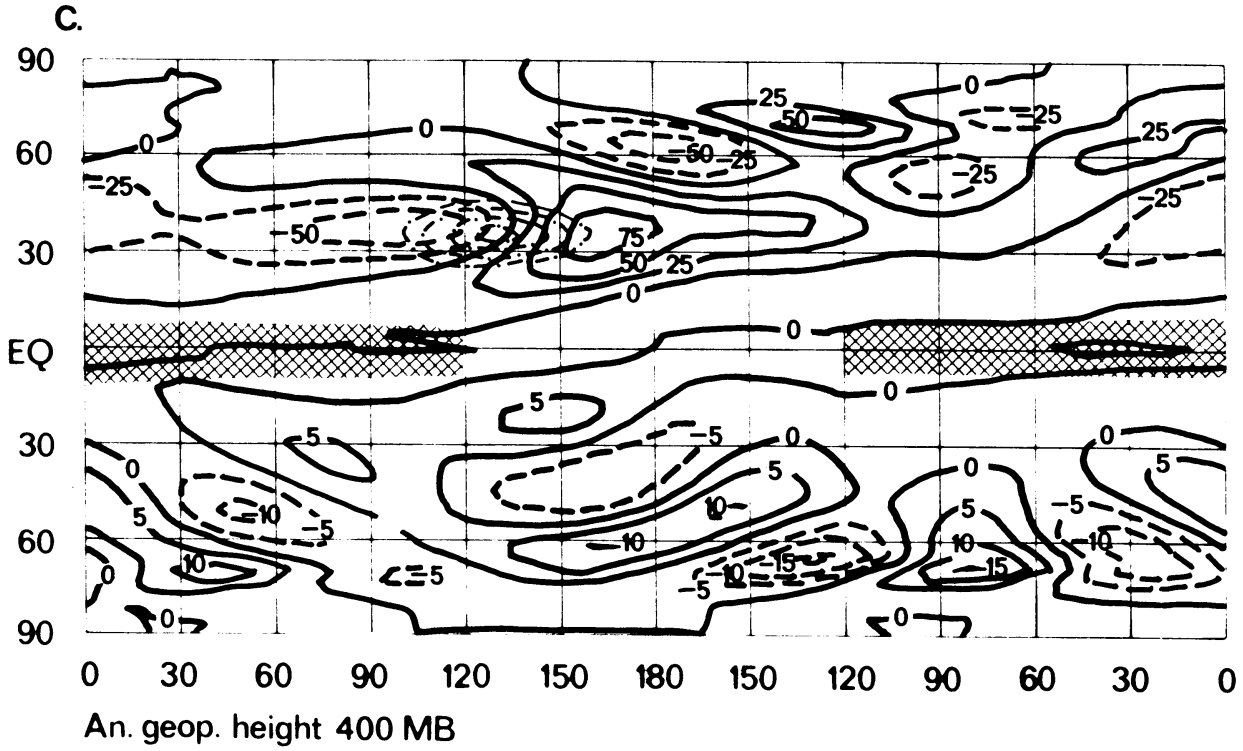
C.
90
60
30
EQ
30
60
90
0 30 60 90 120 150 180 150 120 90 60 30 0
An. geop. height 400 MB

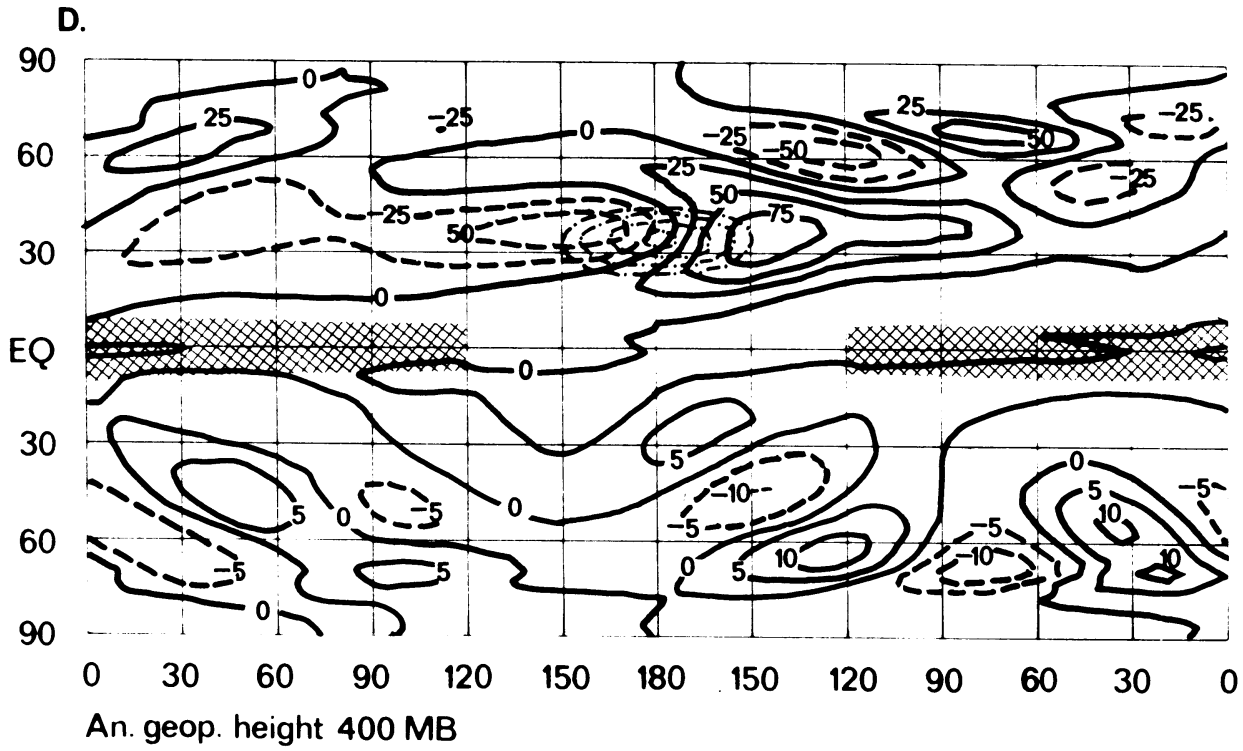
D.
90
60
30
EQ
30
60
90
0 30 60 90 120 150 180 150 120 90 60 30 0
An. geop. height 400 MB

Fig. 5 (cont.)

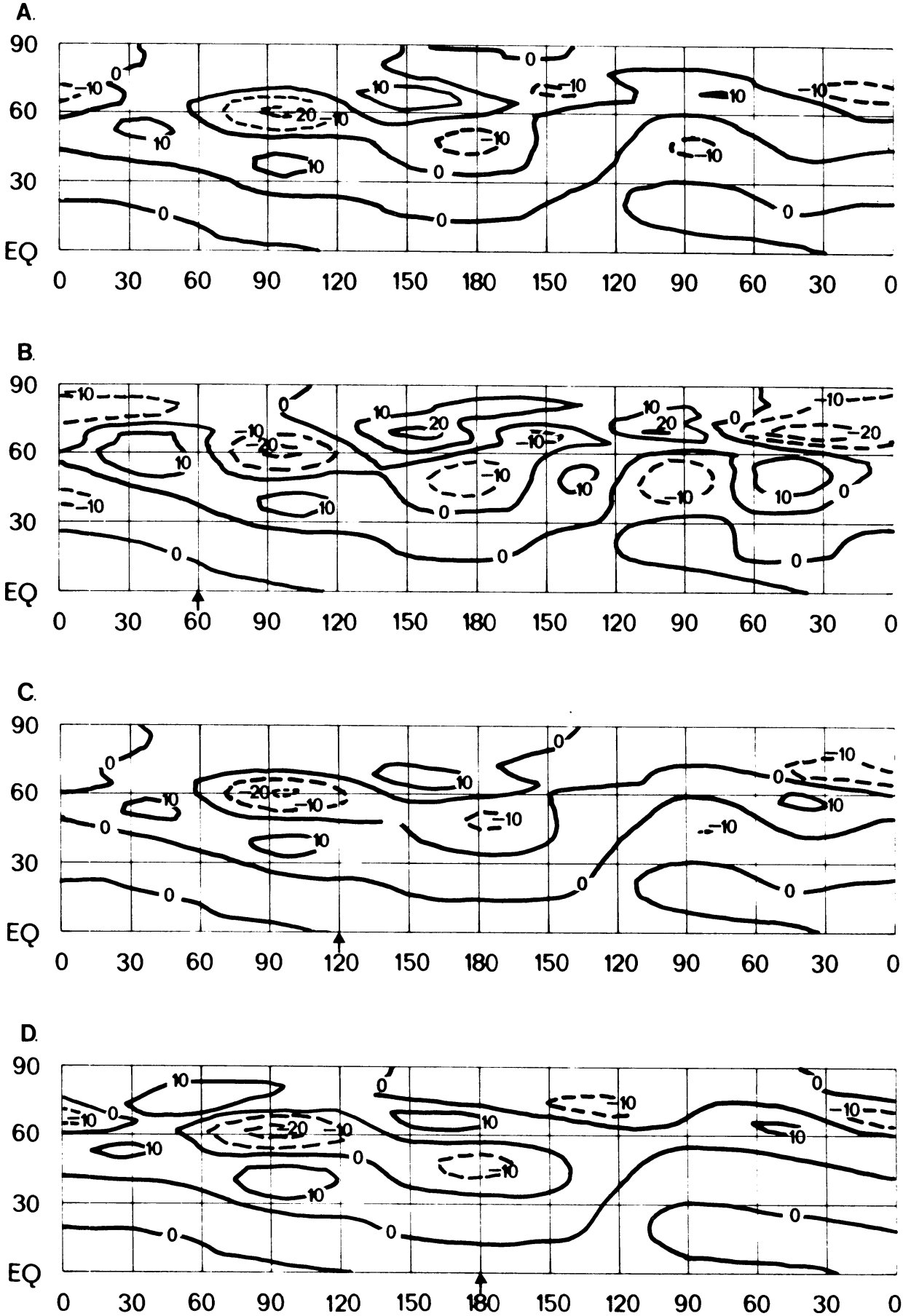

Fig. 6

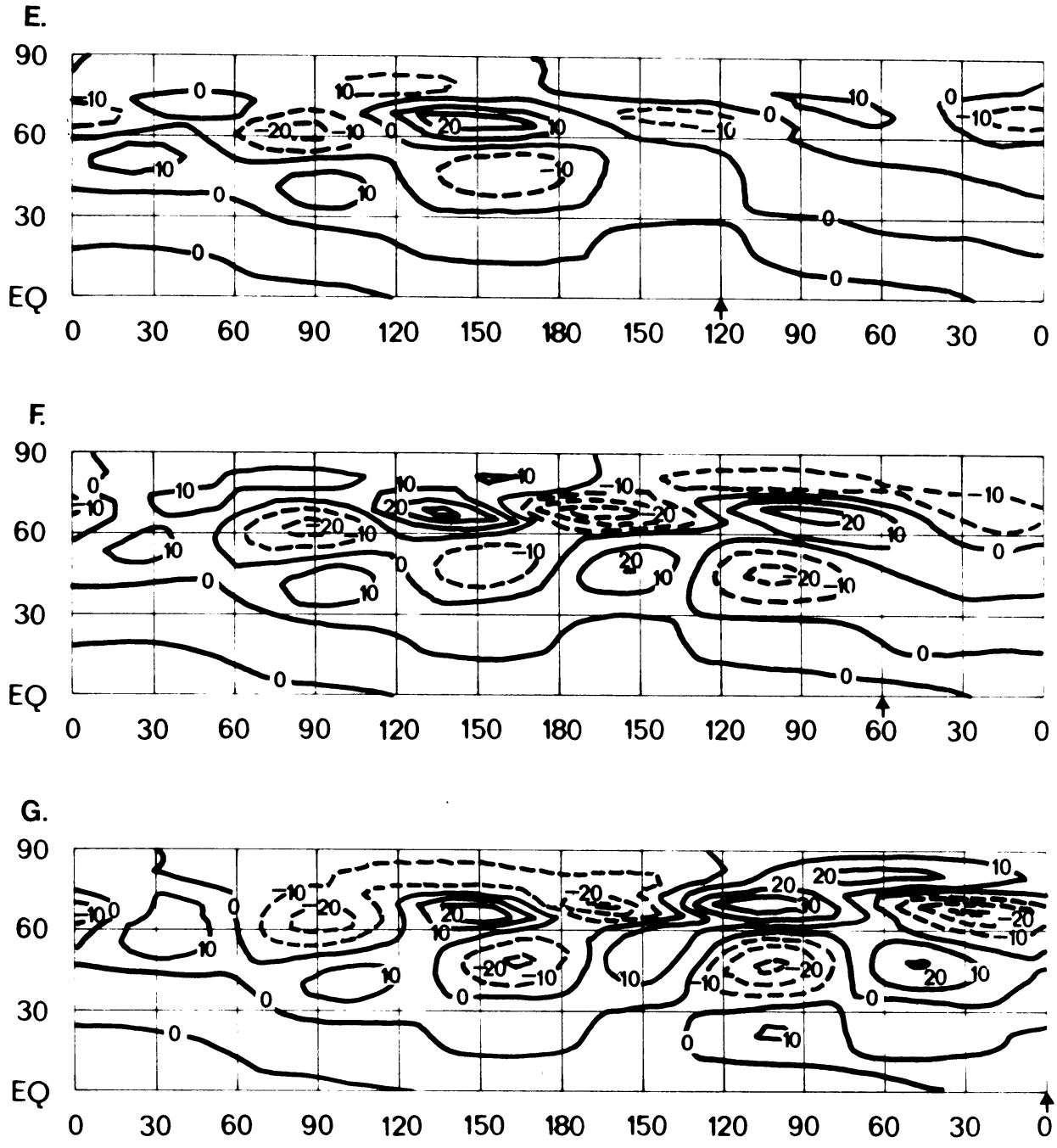
E.
90
60
30
EQ
0 30 60 90 120 150 180 150 120 90 60 30 0
F.
90
60
30
EQ
0 30 60 90 120 150 180 150 120 90 60 30 0
G.
90
60
30
EQ
0 30 60 90 120 150 180 150 120 90 60 30 0

Fig. 6 (cont.)

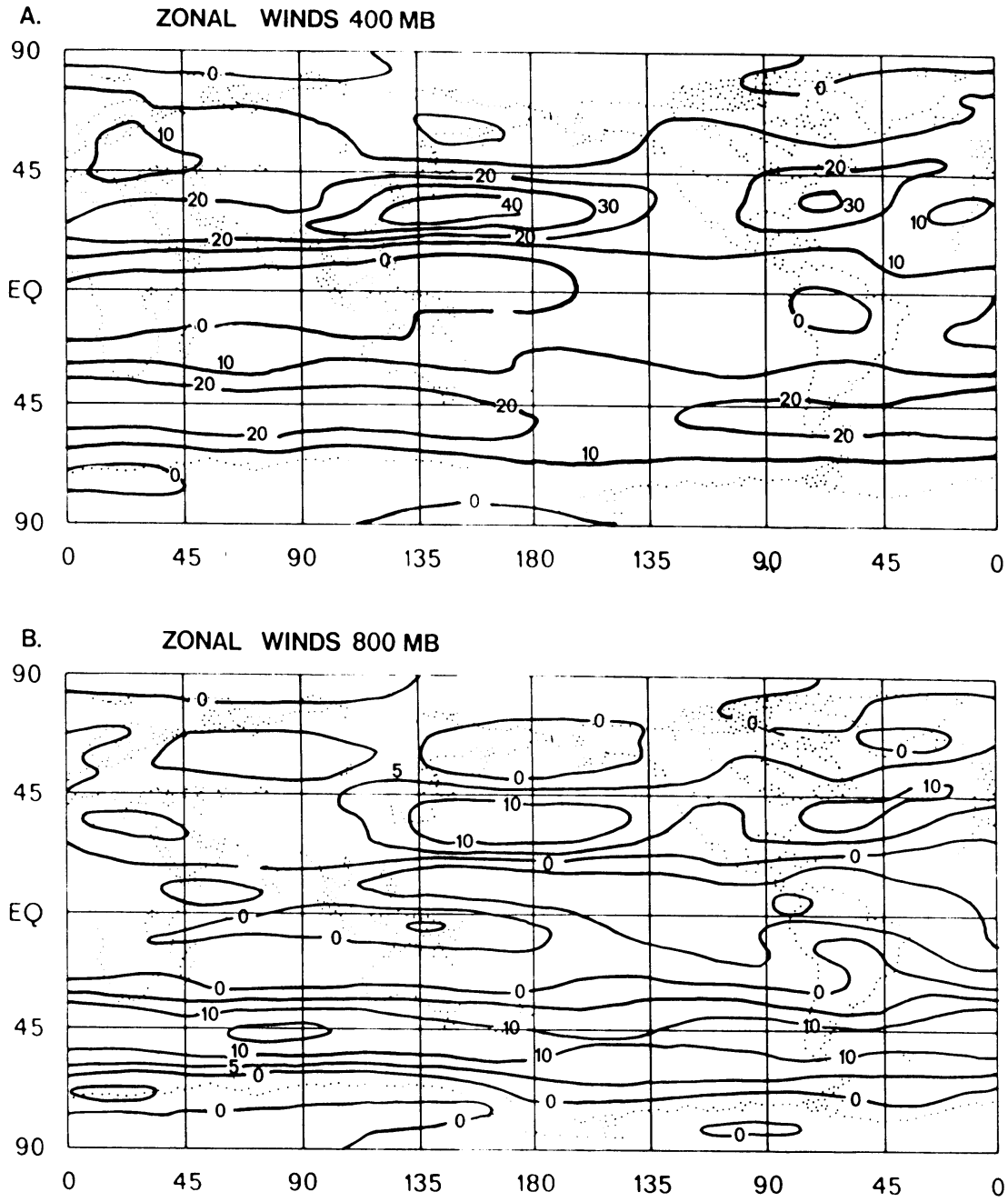
A.
ZONAL WINDS 400 MB
90
45
EQ
45
90
0
45
90
135
180
135
90
45
0
B.
ZONAL WINDS 800 MB
90
45
EQ
45
90
0
45
90
135
180
135
90
45
0

Fig. 7

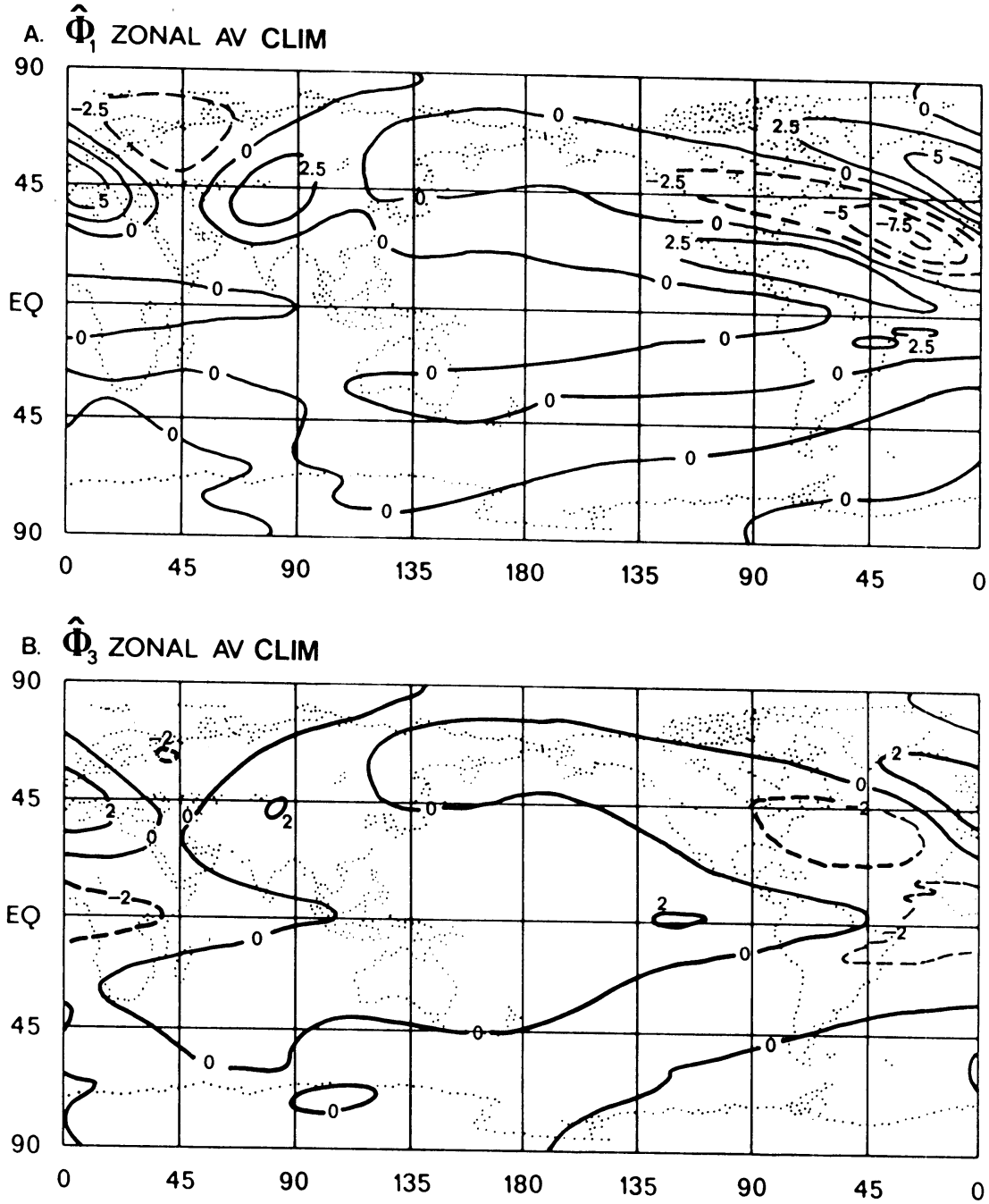
A. $\hat{\Phi}_1$ ZONAL AV CLIM
90
45
EQ
45
90
0
45
90
135
180
135
90
45
0
B. $\hat{\Phi}_3$ ZONAL AV CLIM
90
45
EQ
45
90
0
45
90
135
180
135
90
45
0

Fig. 8

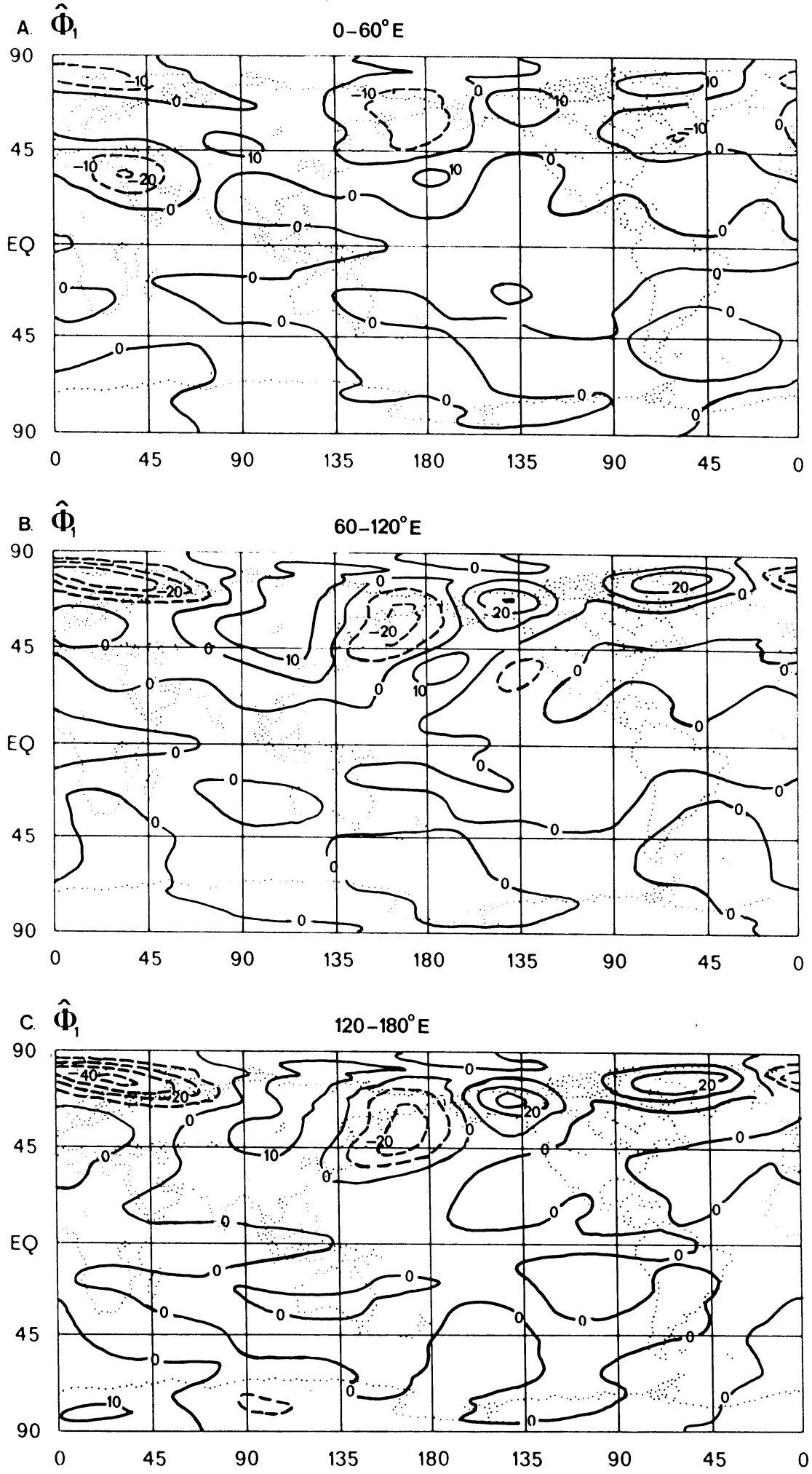
A. $\hat{\Phi}_1$
0–60°E
B. $\hat{\Phi}_1$
60–120°E
C. $\hat{\Phi}_1$
120–180°E
90
45
EQ
45
90
0
45
90
135
180
135
90
45
0

Fig. 9

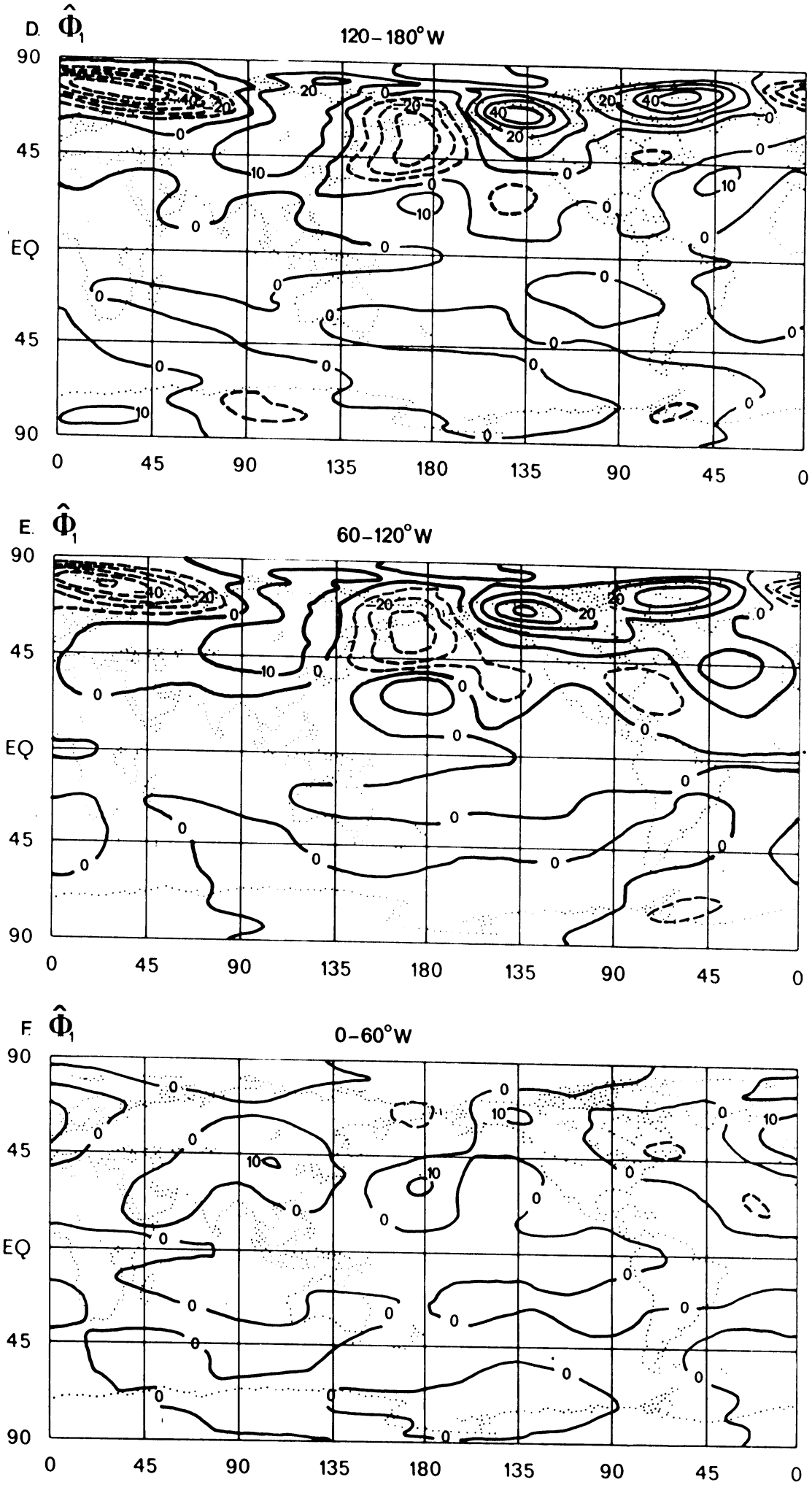
D. $\hat{\Phi}_1$
120–180°W
E. $\hat{\Phi}_1$
60–120°W
F. $\hat{\Phi}_1$
0–60°W
90
45
EQ
45
90
0
45
90
135
180
135
90
45
0

Fig. 9 (cont.)

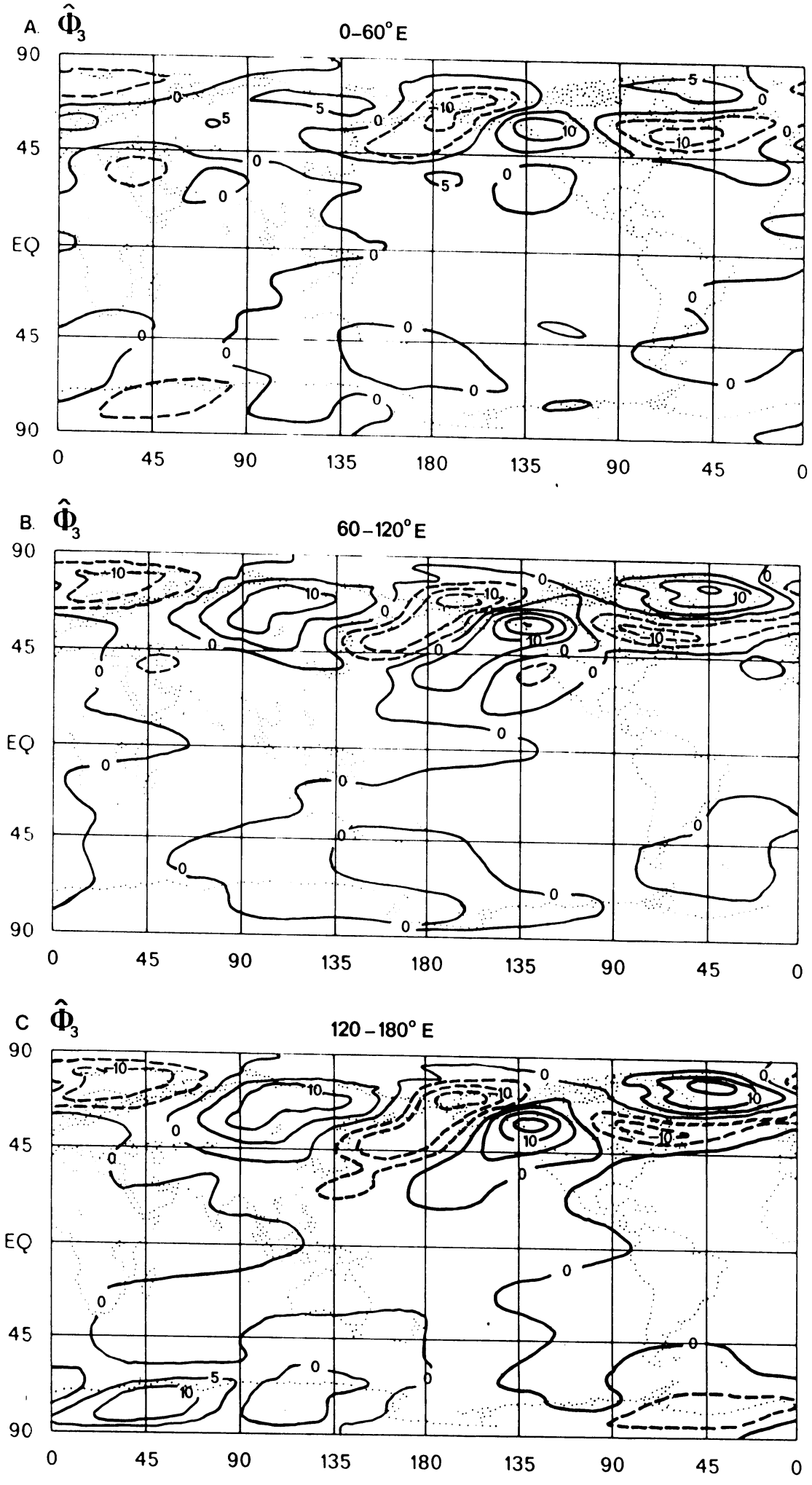
A. $\hat{\Phi}_3$
0-60° E
B. $\hat{\Phi}_3$
60-120° E
C $\hat{\Phi}_3$
120-180° E
90
45
EQ
45
90
0
45
90
135
180
135
90
45
0

Fig. 10

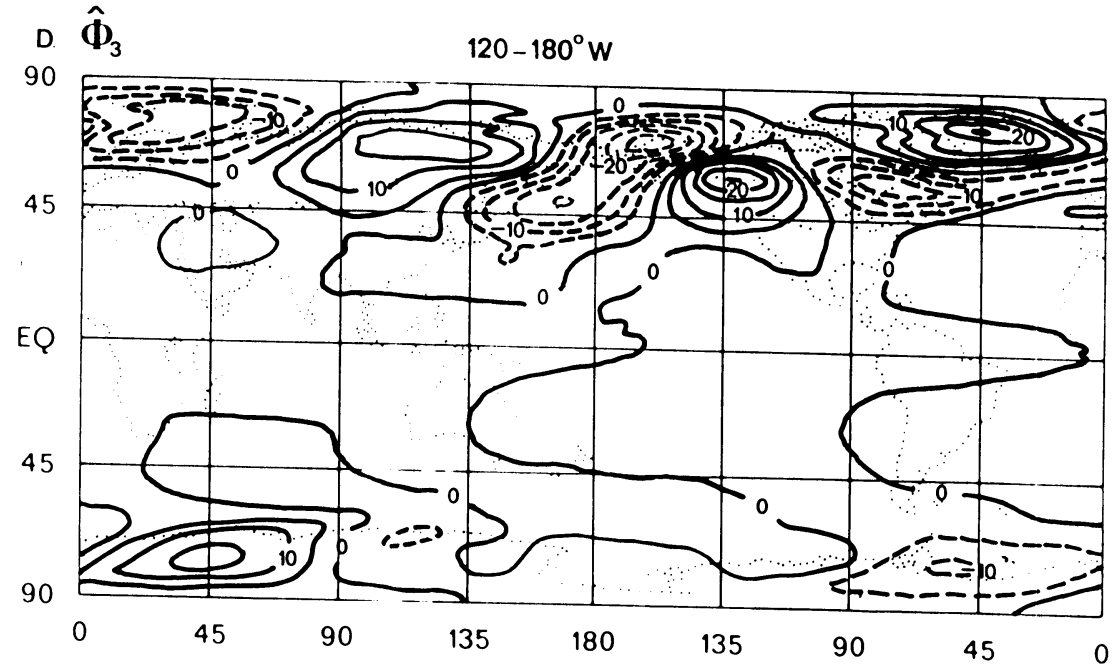
D $\hat{\Phi}_3$
120-180°W
90
45
EQ
45
90
0
45
90
135
180
135
90
45
0

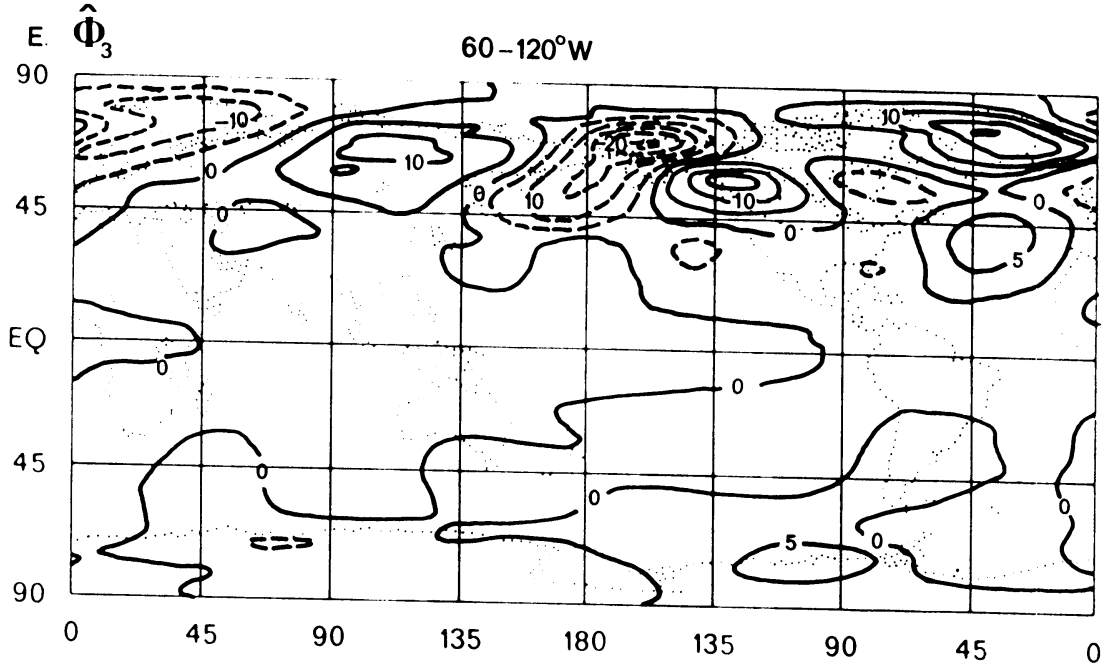
E $\hat{\Phi}_3$
60-120°W
90
45
EQ
45
90
0
45
90
135
180
135
90
45
0

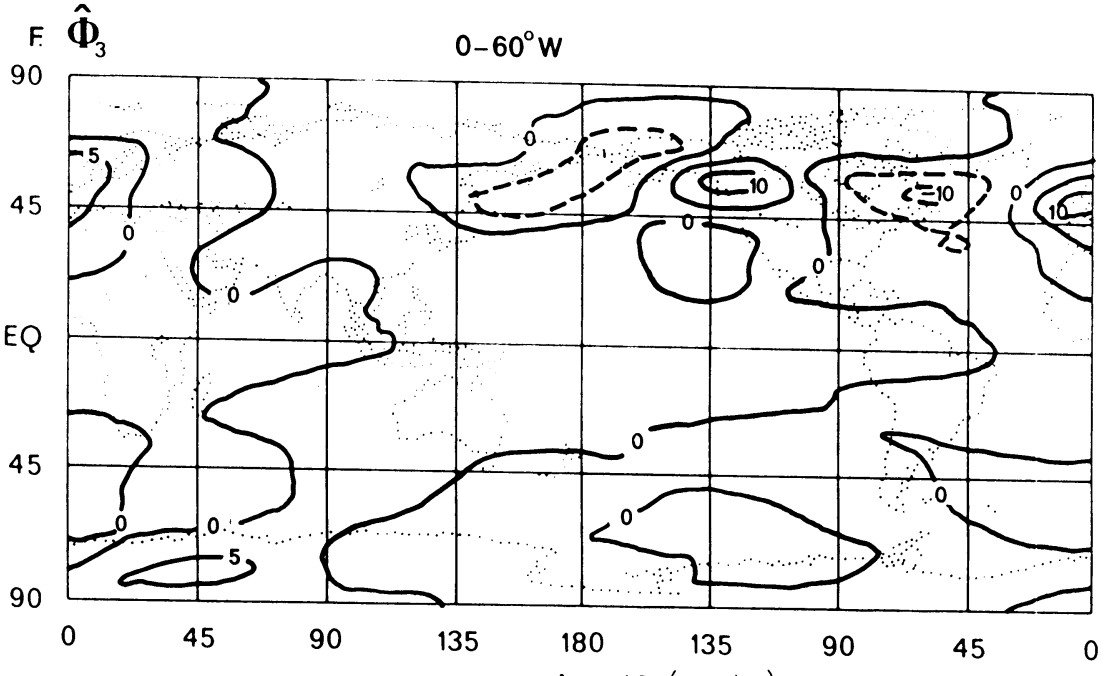
F $\hat{\Phi}_3$
0-60°W
90
45
EQ
45
90
0
45
90
135
180
135
90
45
0

Fig. 10 (cont.)